Review Article

Nano Research
2021, 14(9): 3096–3111

ISSN 1998-0124 CN 11-5974/O4
https://doi.org/10.1007/s12274-021-3490-0

Recent developments of emerging inorganic, metal and carbon-based nanomaterials for pressure sensors and their healthcare monitoring applications

Kyowon Kang[§], Jaejin Park[§], Kiho Kim[§], and Ki Jun Yu (✉)

School of Electrical and Electronic Engineering, YU-KIST Institute, Yonsei University, Seoul 03722, Republic of Korea
[§] Kyowon Kang, Jaejin Park, and Kiho Kim contributed equally to this work.

Received: 6 December 2020 / **Revised:** 30 March 2021 / **Accepted:** 31 March 2021

ABSTRACT

Recently, flexible pressure sensors have gained substantial research interest in bioelectronics because they can monitor the conditions of various organs, enable early diagnosis of diseases, and provide precise medical treatment by applying them to various parts of the body. In particular, inorganic materials, metal and carbon-based materials are broadly used in novel structured pressure sensors from wearable devices to implantable devices. With the excellent electronic properties, distinctive morphologies, and remarkable mechanical and chemical stability of these materials, it is expected that these flexible pressure sensors can be the basis for new methods for human healthcare. This article covers an extensive review of the inorganic, metal and carbon-based flexible pressure sensor design strategies and sensing mechanisms studied in recent years for diverse applications such as tactile sensors, arterial pulse sensors, intracranial pressure sensors, intraocular pressure sensors, and bladder pressure sensors. Each section provides an overview by introducing the recent progress in flexible pressure sensors.

KEYWORDS

nanomaterial, inorganic, carbon, pressure sensor, wearable device, implantable device

1 Introduction

As the rapid development of flexible pressure sensors is changing the mode of medical devices, there is an increasing demand for pressure sensors that can be used in a variety of applications. Recently, real-time monitoring pressure sensors have been reported that measure health-related signals, such as respiration rate, pronunciation, intracranial pressure, intraocular pressure, and blood flow, and external stimuli for tactile sensing [1–5]. They have huge potential in daily health monitoring systems because these devices provide clinically critical information for the early detection of diseases and enable the capture of body activities or mimicking of touch perception/gestures. To improve the performance of pressure sensors, it is important to consider important characteristics of the sensors such as the sensitivity, response time, proper sensing range, flexibility, stretchability, light weight, and human-friendly imperceptible use in daily healthcare systems [6–15].

There have been great efforts to enhance these performance parameters, which can be realized by designing unique nano/microstructures and utilizing various materials, including inorganic materials, carbon-based materials, polymers, and metals. To improve these parameters, it is important to understand the mechanism of a typical pressure sensor; that is, external pressure results in deformation of the structure and changes in electrical properties, which are indicators for quantifying the magnitude of mechanical stimuli. High-sensitivity, miniaturized, compatible, skin-attachable sensors can be achieved by controlling the nano/microscale morphologies of suitable materials such as inorganic materials or carbon-based materials [16–18]. The inorganic materials and metals have high mechanical stability and excellent electrical properties in the form of nanoparticles, nanowires or nanomembranes, thereby being utilizable as novel pressure sensors [19]. Advanced carbon materials have high conductivity and stability, but they are toxic when directly applied to human organs without other treatments. Therefore, carbon materials are usually combined with suitable encapsulants for long-term stable performance with less toxicity and flexibility [20]. By using these novel materials, wearable or implantable pressure sensors can be applied to various medical devices as shown in Scheme 1. Wearable pressure sensors are attached to the skin or robotics for sensing healthcare biophysical signals or realizing tactile perception. Implantable pressure sensors are used for measuring very small changes in pressure, such as in intracranial or intraocular pressure. These wearable/implantable pressure sensing devices and noninvasive pressure sensors are necessary for future healthcare devices with novel features that can be acquired via functional materials and innovative design structures.

This paper summarizes the applications of and developments in flexible pressure sensors fabricated with inorganic materials, metals and carbon-based materials to detect physical activities from the human body as well as external stimuli. We review pressure sensors based on their structure, working mechanism, unique features that can provide wearable or implantable

Address correspondence to kijunyu@yonsei.ac.kr

sensing capability and biocompatibility. Furthermore, various applications of flexible pressure sensors for detecting biophysical signals or realizing tactile sensing are introduced in each section. Finally, this paper aims to provide a wide overview of wearable/ implantable pressure sensors composed of inorganic materials, metals and carbon-based materials for next-generation healthcare systems.

2 Inorganic material and metal-based pressure sensors

Inorganic materials and metals, such as nanowires [21–23], nanoparticles [24, 25], nanomembranes [26], and semiconducting nanomaterials, have great potential in various fields due to their high electrical mobility, remarkable stability, and superior sensitivity [27–29]. Due to these outstanding properties, inorganic materials and metals have been applied to a wide range of high-performance devices that are utilized not only as conventional electronics but also in medical applications [30–38]. Since measuring the pressure from the human body is important from healthcare monitoring and medical treatment aspects, development of pressure sensors has gained substantial interest. In this section, we introduce recent progress in developing novel inorganic and metal-based pressure sensors by reviewing their performance, material properties, and unique applications.

2.1 Inorganic material and metal-based wearable pressure sensors

Wearable electronics have received significant attention and grown rapidly in recent years because of their excellent mechanical stretchability and excellent electrical performance such that they can be utilized for various applications in healthcare systems such as wearable healthcare monitors, electronic skins, prosthetic skins, and touch interfaces [39–44]. A pressure sensor that utilizes a wearable platform should be attached to the skin to measure external pressure or physiological signals, such as body movement, arterial pulse, respiration and phonation, under continuous monitoring without any noise to show high performance. Therefore, thinness and flexibility of sensors are necessary to form conformal contact with the human body when the devices are used for healthcare monitoring. Over the past decade, researchers have studied inorganic materials and metals such as nanomembranes [32, 33], nanowires [34, 35, 45–47] and nanoparticles [48] for wearable sensors. They are used as novel flexible pressure sensors because of their high electrical mobility, remarkable stability, and low degradation on human skin. This section describes the principles and applications of measuring various pressures by integrating inorganic materials or metals with a flexible device on the human body. The characteristics and performances of the inorganic and metal-based wearable pressure sensors are compared in Table 1.

2.1.1 *Inorganic material and metal-based tactile sensors*

Flexible and wearable tactile sensors based on inorganic materials/ metal and soft elastomeric substrates that can be intimately attached to the skin have received substantial interest for developing high-performance sensors with good sensitivity and mechanical stability. Their superior potential can expand promising applications such as human–machine interactions, artificial electronic skins, and smart wearable equipment.

Figure 1(a) shows a highly sensitive (~ 3.8 kPa^{-1}) and flexible

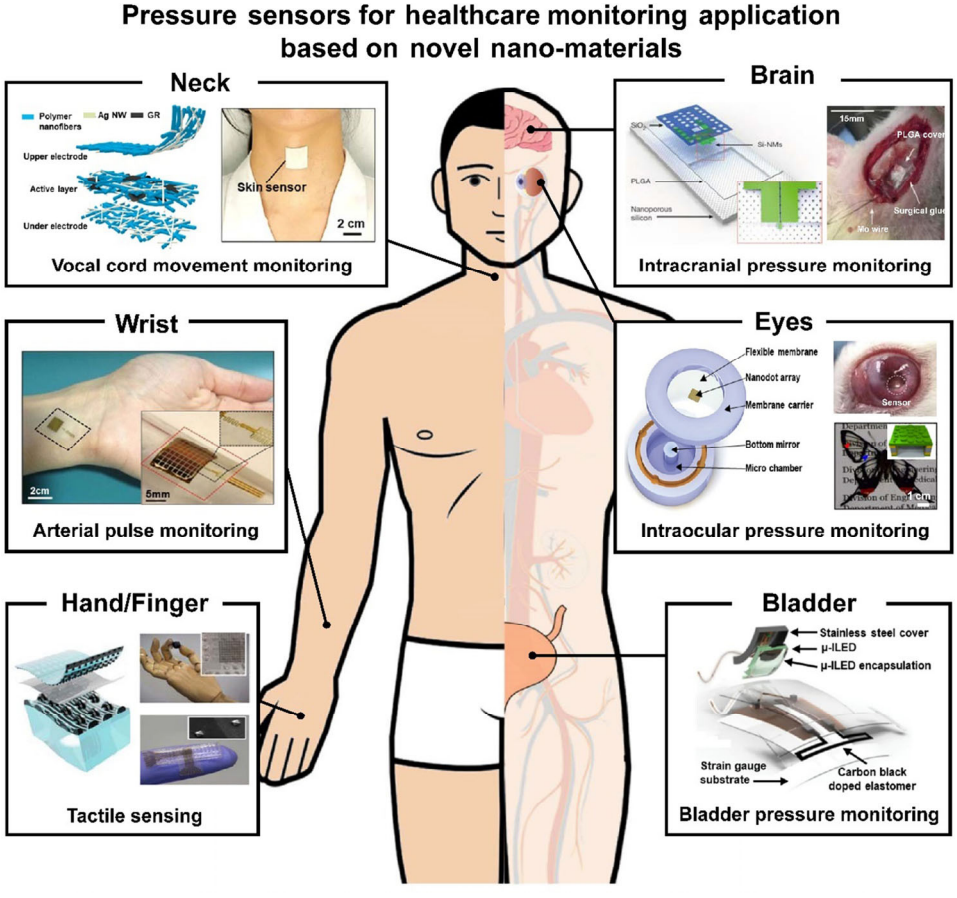

Scheme 1 Pressure sensors for healthcare monitoring application based on novel nano-materials. Reproduced with permission from Ref. [32, 35, 102, 120, 129], © Macmillan Publishers Limited 2014, American Chemical Society 2020, Macmillan Publishers Limited 2016, Lee, J. O. et al. 2017, Boutry, C. M. et al. 2018, and Springer Nature Limited 2019, respectively.

Table 1 The characteristics and performances of the inorganic material and metal-based wearable pressure sensors

Material	Type	Pressure range	Sensitivity	Response time	Reference
AgNW-embedded PDMS	Piezocapacitive	< 500 Pa/2.5 kPa	3.8 kPa^{-1}/0.8 kPa^{-1}	150 ms	[45]
AgNWs/tissue paper	Piezoresistive	< 30.2 kPa	1.5 kPa^{-1}	90 ms	[46]
AuNWs/tissue paper	Piezoresistive	< 0.5 kPa	1.14 kPa^{-1}	17 ms	[47]
SSNP/PU	Piezoresistive	< 1 kPa	2.46 kPa^{-1}	30 ms	[48]
PZT	Piezoelectric	—	—	0.1 ms	[32]
PZT thin film	Piezoelectric	< 30 kPa	0.018 kPa^{-1}	60 ms	[33]
v-AuNWs/PDMS	Piezoresistive	< 600 Pa/> 600 Pa	23 kPa^{-1}/0.7 kPa^{-1}	10 ms	[34]
AgNWs/GR/PANF	Piezoresistive	< 1.5 kPa/75 kPa	134 kPa^{-1}/0.7 kPa^{-1}	20 ms	[35]

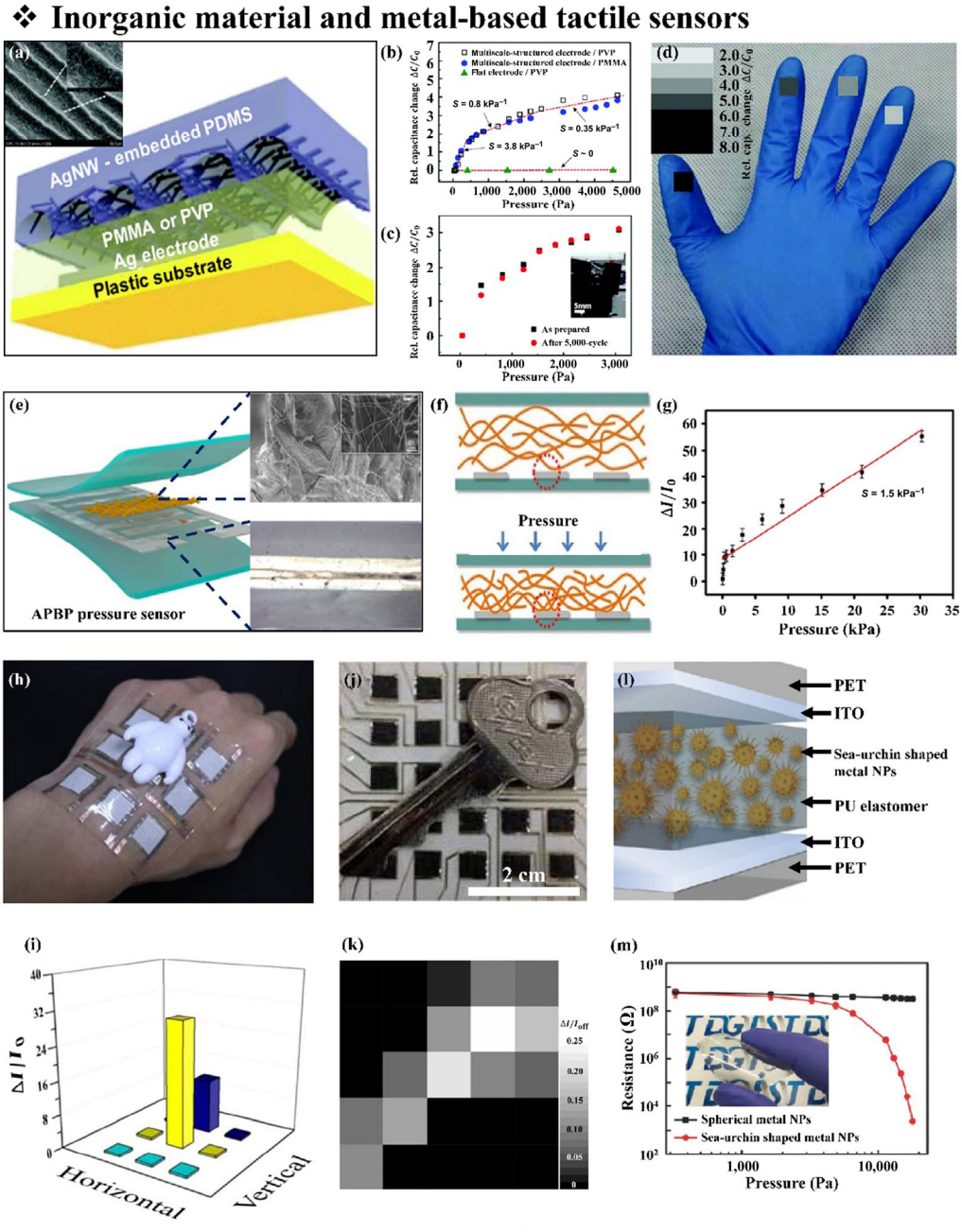

Figure 1 Inorganic material and metal-based tactile sensors. (a) Schematic of a capacitive pressure sensor with a multiscale-structured elastomeric electrode; the inset shows an SEM image. (b) Relative capacitance change–pressure curve of the multiscale-structured elastomeric electrode. (c) Bending stability of (a) after a 5,000-cycle bending test. (d) Fingertip grip pressure sensing while grabbing a plastic cup. Reproduced with permission from Ref. [45], © The Royal Society of Chemistry 2015. (e) Schematic of an APBP pressure sensor, the insets show the AgNWs/tissue paper and interdigitated electrodes. (f) Working mechanism of the APBP sensor. (g) Current response–pressure curve of the APBP sensor. (h) and (i) Performance of APBP sensor arrays. Reproduced with permission from Ref. [46], © American Chemical Society 2019. (j) and (k) Performance of AuNW-embedded pressure sensor arrays. Reproduced with permission from Ref. [47], © Macmillan Publishers Limited 2014. (l) Schematic of an SSNP-based pressure sensor. (m) Piezoresistive characteristics of pressure sensors using SSNPs and spherical nanoparticles, the inset shows a photograph of the SSNP-based pressure sensor. Reproduced with permission from Ref. [48], © WILEY-VCH Verlag GmbH & Co. KGaA, Weinheim 2016.

capacitive pressure sensor with a multiscale-structured elastomeric electrode [45]. Using a prestrained polydimethylsiloxane (PDMS) mold, a silver nanowire (AgNW)-embedded multiscale-structured PDMS electrode is fabricated (Fig. 1(a) inset). Through a solution process using polymethylmethacrylate (PMMA) or polyvinylpyrrolidone (PVP) as a dielectric layer, a flexible capacitive pressure sensor is obtained. Figure 1(b) shows the difference in performance between the multiscale-structured electrode and the non-structured flat electrode. Additionally, the former shows no considerable degradation for 5,000 bending cycles (Fig. 1(c)). Figure 1(d) shows fingertip grip pressure sensing and the corresponding relative capacitance changes while grabbing a plastic cup with four fingertips. A highly sensitive and flexible capacitive pressure sensor with low-cost fabrication may widen its application to wearable electronic skins.

A low-cost and simple fabrication process is also an important factor to be considered when manufacturing a tactile sensor. Figure 1(e) shows an all paper-based piezoresistive (APBP) pressure sensor with low-cost, facile manufacturing advantages [46]. The APBP pressure sensor is composed of silver interdigitated electrodes printed by a direct writing method (Fig. 1(e) top inset) and tissue paper with a porous structure and a rough surface as a sensing material coated with AgNWs by a dip-drying method (Fig. 1(e) bottom inset). The working mechanism of the APBP is shown in Fig. 1(f). When external pressure is applied, the number of conductive microfibers in contact with interdigitated electrodes increases due to the compression deformation of the tissue paper, increasing the conductive pathways. The performance of the APBP pressure sensor is about 1.5 kPa^{-1}, which is indicated in Fig. 1(g). Figures 1(h) and 1(i) show that the APBP pressure sensor works as a tactile sensor when attached to the skin. Additionally, gold nanowire (AuNW) can be utilized as a tactile sensor, which can be obtained by sandwiching ultrathin AuNW-impregnated tissue paper between two flexible PDMS sheets [47]. Figures 1(j) and 1(k) show the detection of an object through a AuNW-embedded flexible tactile sensor array. These devices enable an efficient, low-cost fabrication strategy using metal nanowires and tissue paper to construct a highly sensitive, flexible pressure sensor.

Metal nanoparticles are also being studied for flexible pressure sensors as much as metal nanowires. Figure 1(l) shows the structure of a highly sensitive, transparent, and flexible tactile sensor composed of sea-urchin-shaped metal nanoparticles (SSNPs) and insulating polyurethane (PU) elastomer [48]. It shows outstanding pressure sensing performance due to the effective quantum tunneling effect among SSNPs in the PU elastomer. Figure 1(m) shows the difference in the performance of the pressure sensor using SSNPs and the pressure sensor using spherical metal nanoparticles without spikes. The former also exhibits superior optical transmittance (84.8% at 550 nm), as shown in the inset of Fig. 1(m), which has great advantages from the aesthetic aspect.

2.1.2 *Inorganic material and metal-based physiological signal sensors*

Continuous monitoring of physiological signals, such as the arterial pulse, respiration and pronunciation, using pressure sensors attached to the skin is an important technique for detecting the initial occurrence of cardiovascular disease and evaluating the patient's health condition, early disease warning signs and treatment methods. Various inorganic materials and metals have been studied to develop flexible physiological signal sensors that can exhibit ultrathin and ultrasensitive properties.

Lead zirconate titanate ($Pb[Zr_xTi_{1-x}]O_3$, PZT) is a typical piezoelectric material for pressure sensors due to its large piezoelectricity, excellent electromechanical coupling coefficients and high dielectric permittivity. Figure 2(a) shows a piezoelectric pressure sensor based on PZT [32]. To detect weak physiological signals, the authors used a silicon nanomembrane (SiNM) n-channel metal-oxide-semiconductor field effect transistor (MOSFET), which can amplify the piezoelectric voltage response of PZT and convert it to a current output through capacitance coupling. Figure 2(b) shows blood pressure wave measurements with the device attached to the wrist, and Fig. 2(c) displays an extension of the dashed box in Fig. 2(b). The peak labeled P_1 is the sum of the incident wave and reflected wave from the hand, and P_2 is the difference between the reflected wave from the lower body and end-diastolic pressure. This indicates the feasibility of using flexible devices based on PZT to measure subtle signals on the human body.

It is also very important that the physiological signal sensor does not restrict the patient's movement when monitoring the patient's health condition. Figure 2(d) shows a self-powered flexible piezoelectric pressure sensor based on a PZT thin film to enable *in vivo* measurement of physiological signals with a wireless signal transmission system [33]. The inorganic PZT piezoelectric sensor on ultrathin polyethylene terephthalate (PET) can respond to subtle pulse changes occurring on the epidermis through conformal contact with the skin. Figure 2(e) presents the performance of the sensor, with a sensitivity of ~ 0.018 kPa^{-1} and a response time of ~ 60 ms, and carotid artery pulse measurement is shown in Fig. 2(f).

Researchers have made efforts to increase the sensitivity of pressure sensors by developing novel structures. Figure 2(g) shows conformal coating of vertically aligned gold nanowires (v-AuNWs) on arranged pyramid microarrays on PDMS [34]. The pressure sensing mechanism can be attributed to the geometrical contact area changes at the interface between v-AuNWs/PDMS microarrays and the interdigitated electrodes under applied pressure. The hierarchical v-AuNWs/PDMS structured flexible pressure sensor exhibits high performance, as shown in Fig. 2(h). At low pressure (< 600 Pa), the sensor presents a high sensitivity of S_{p_1} = 23 kPa^{-1}. Real-time wrist pulse wave monitoring with a physiological signal sensor based on v-AuNW is shown in Fig. 2(i), which may be scalable for future applications in remote health condition monitoring.

Figure 2(j) shows an ultrathin, high-performance wearable pressure sensor, which is composed of hierarchically mesh-shaped pressure-sensitive materials and electrodes [35]. The pressure-sensitive material is composed of AgNWs, graphene (GR), and polyamide nanofibers (PANFs). A high proportion of AgNWs are embedded in a PANF network, acting as enhanced conductive pathways. Additionally, the graphene bridges the crossed AgNWs, and the PANFs mainly protect the AgNWs/GR as a supporting mesh-shaped structure. Figures 2(k) and 2(l) shows a sensor attached to the neck to detect vocal cord movement when speaking any sentence.

2.2 Inorganic material-based implantable pressure sensors

In modern clinics, it is important to monitor the pressure induced by various organs because it is an indicator for diagnosis of diseases and monitoring the condition of the organs. Non-invasive monitoring methods that use light and X-rays to sense the pressure of the target area have been widely explored [49–52]. However, non-invasive methods monitor pressure indirectly, which has lower accuracy than direct monitoring methods. Therefore, to measure bio-signals more

❖ Inorganic material and metal-based physiological signal sensors

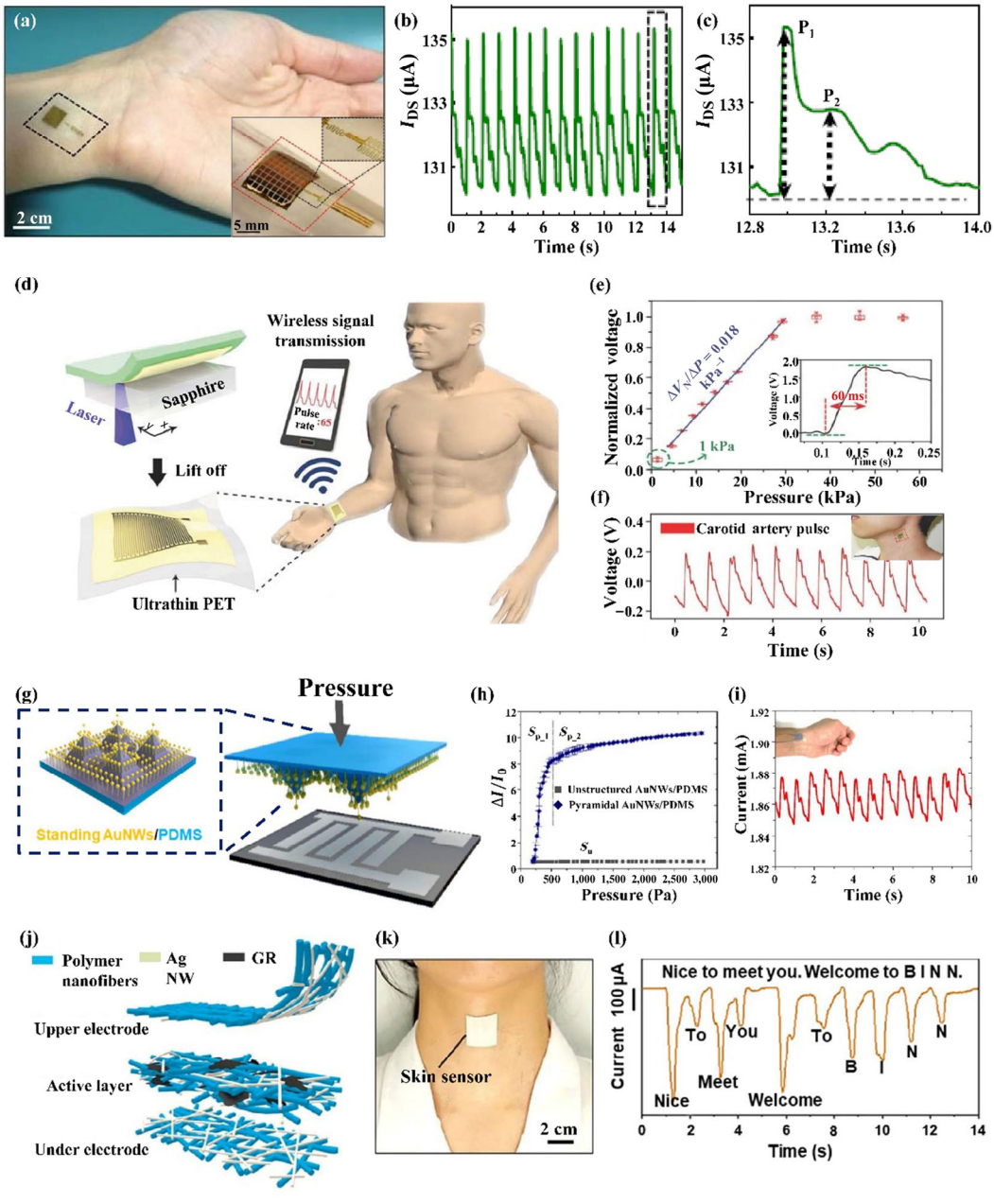

Figure 2 Inorganic material and metal-based physiological signal sensors. (a) Photograph of a PZT-based pressure sensor laminated on a wrist and a device, the inset shows wrapped on a cylindrical glass support. (b) I_{DS}–time plot of the sensor mounted on the wrist. (c) I_{DS}–time plot for data in the region indicated by the dashed box in (b). Reproduced with permission from Ref. [32], © Macmillan Publishers Limited 2014. (d) Schematic illustration of the fabrication process for the self-powered pressure sensor and wireless transmission of detected pulse signals to a smart phone. (e) Normalized output voltage as a function of pressure. The inset shows the enlarged output peak representing the response time of the pressure sensor. (f) Output voltage generated in response to the carotid artery pulse. Reproduced with permission from Ref. [33], © WILEY-VCH Verlag GmbH & Co. KGaA, Weinheim 2017. (g) Schematic of a hierarchical v-AuNWs/PDMS structured flexible pressure sensor. (h) Pressure–response curves of the pyramidal and unstructured AuNWs/PDMS films. (i) Real-time current–time curve of the sensor. Reproduced with permission from Ref. [34], © American Chemical Society 2019. (j) Schematic of a Ag NWs/GR/PANF pressure sensor with Ag NWs nanonetwork electrodes. (k) and (l) Photograph of the pressure sensor attached to the throat and response curves when the wearer spoke any sentence. Reproduced with permission from Ref. [35], © American Chemical Society 2020.

precisely, the most accurate way is to implant the sensors directly into the target organ. Representative examples of implantable electronics include chronically implantable electronics [27, 53–59] and transient/biodegradable electronics [60–67]. Chronically implantable electronics can be directly implanted over the target area of the organs and operate indefinitely in the body without any performance degradation. On the other hand, transient electronics, which dissolve in the body after the programmed operational period, reduce the risk of an inflammatory response from long-term implantation. Since transient electronics are biodegradable, an additional post-operation for removing the device after device operation is unnecessary. The lifetime of transient electronics depends on certain circumstances such as the pH, temperature, thickness of the materials, and types of encapsulation materials such as silicon nanomembrane, polyanhydride [68–74]. The characteristics and performances of the inorganic material-based implantable pressure sensors are compared in Table 2.

Table 2 The characteristics and performances of the inorganic material-based implantable pressure sensors

Material	Type	Pressure range	Sensitivity/accuracy	Reference
SiNM encapsulated with SiO_2	Piezoresistive	< 100 mmHg	50 Ω/mmHg	[61]
SiNM encapsulated with SiMM/wax	Piezoresistive	< 100 mmHg	17.3 Ω/mmHg	[62]
Mg/air/Zn	Inductive-capacitive	< 79 mmHg	200 kHz/mmHg	[63]
Au nanodot array	Near-infrared (NIR) light reflection	< 40 mmHg	0.29 mmHg	[102]
Si_3N_4/b-Si	NIR light reflection	< 40 mmHg	0.58 mmHg	[103]
Nanostructured Si_3N_4	NIR light reflection	< 32 mmHg	0.07 mmHg	[104]

2.2.1 *Inorganic material-based intracranial pressure sensors*

In modern clinical medicine, monitoring the intracranial pressure (ICP) is important for proper medical treatment of brain diseases from hydrocephalus and stroke to traumatic brain injury. Monitoring the ICP can allow one to determine accurate treatment, which reduces the rate of morbidity and enhances recovery. The ICP is the pressure of the cerebrospinal fluid (CSF) located between the brain and the skull. Therefore, sensing the pressure instead of the strain, which is a biaxial force, is more effective in monitoring the ICP [60, 62, 63, 75, 76]. Pressure can be measured by various methods, but commonly used methods involve sensing the resistance change according to the deformation of the sensing layer when pressure is applied or the capacitance difference due to the deformation of the insulator layer located between two electrodes.

Single-crystalline SiNMs are one of the common materials that have piezoresistive characteristic [60, 77–79]. When strain is applied, due to the piezoresistive effect, the energy band of silicon shifts, inducing changes in the bandgap. This causes carrier redistribution, which results in a change in the effective mass and mobility. Since the piezoresistive effect governs other effects, such as a geometrical effect of multiple magnitudes, silicon-based strain sensors have a much higher gauge factor (~ 100) than conventional metal-based strain sensors (~ 2). With a strain sensor, pressure can be measured by applying the "reservoir structure" or "air-cavity structure". Figure 3(a) shows the SiNM-based transient ICP sensor with an air-cavity structure [61]. The SiNM is patterned in a serpentine structure to enhance the sensitivity and stretchability at the same time. The air-cavity structure is located under the silicon nanomembrane and a stretchable poly(lactic-co-glycolic acid) (PLGA) substrate. When external pressure is applied to the sensor, the strain is concentrated on the edge of the air cavity and SiNM (Fig. 3(a) top inset). The SiO_2 layer serves as a passivation and transient encapsulation layer. The whole device is composed of transient materials so that after a programmed period of operation, the device will biodegrade; thus, postoperative removal of the device is not required (Fig. 3(b)). Figure 3(c) shows the monitored ICP of a rat for three days, which is similar to the conventional ICP sensor results.

Hydrolysis by a biofluid occurs on the surface of an implanted biodegradable sensor due to degradation of the encapsulation layer [74, 80–82], which changes the thickness, and a neutral mechanical plane shift occurs. Additionally, biofluids can penetrate traditional bioresorbable electronics through the edge of the device where encapsulation is absent. This penetration causes serious performance degradation of the device and increases noise. To overcome these shortcomings of biodegradable electronics, recent research has presented biodegradable ICP sensors that have constant sensitivity during the degradation process [62]. In addition, by sealing the whole device, including the edges, with biodegradable natural wax, penetration of biofluids has been completely blocked (Fig. 3(d)). A defect-free monocrystalline silicon micromembrane (SiMM) is used as the top encapsulation layer, and the side of the device is sealed with a mixture of natural waxes: Beeswax and Candelilla wax. The sensitivity of the device can be expressed by the following equation.

$$\frac{\bar{\sigma}}{\Delta P} \propto \left[\frac{1 - 2\frac{z_{\text{sensor}}}{h_{\text{PLGA}}} + \left(2 - 2\frac{z_{\text{sensor}}}{h_{\text{PLGA}}}\right)\frac{E'_{\text{Si}} h_{\text{encap}}}{E'_{\text{PLGA}} h_{\text{PLGA}}}}{1 + 4\frac{E'_{\text{Si}} h_{\text{encap}}}{E'_{\text{PLGA}} h_{\text{PLGA}}}} \right]$$

where $E'_{\text{PLGA}} = \frac{E_{\text{PLGA}}}{1 - \nu^2_{\text{PLGA}}}$, $E'_{\text{Si}} = \frac{E_{\text{Si}}}{1 - \nu^2_{\text{Si}}}$, and E_{Si}, E_{PLGA}, ν_{Si}, and ν_{PLGA} are the moduli and Poisson's ratio of Si and PLGA. When the ratio of z_{sensor} (height of SiNM) to h_{PLGA} (thickness of PLGA) is 1/3, the sensitivity is linearly proportional to the constant value. When fabricating the device with a ratio ($z_{\text{sensor}}/h_{\text{PLGA}}$) of 1/3, the results are identical to the finite element analysis (FEA) simulation data (Figs. 3(e) and 3(f)). A movement test of rats indicates that the biodegradable ICP sensor can monitor the ICP sensitively without any performance degradation compared to the commercial ICP sensor.

To measure the pressure, not only piezoresistive materials such as SiNM but also capacitance changes due to the deformation of the insulator layer are used. According to recent research, a bioresorbable wireless pressure sensor has been introduced (Fig. 3(h)) [63]. When external pressure is applied, the thickness of the insulator layer changes, which induces a capacitance difference, the inductor coil converts the capacitance to the resonant frequency, and the converted frequency is wirelessly delivered to the reader. By insulating the edge of the active pressure sensing region with natural wax and air, the parasitic capacitance effect and noise have been dramatically reduced, and the sensitivity has been increased substantially. Figure 3(i) indicates that the noise that occurs during ICP monitoring is negligible when used for clinical purposes. Since the simulation results of the frequency change according to the pressure difference are identical to the sensor results, the pressure sensor functions successfully (Figs. 3(j)–3(l)). However, the device performance can be significantly improved by enhancing the adhesion strategy between the device and target organ surface [83–100].

2.2.2 *Inorganic material-based intraocular pressure sensors*

Many eye-related diseases, such as glaucoma and cataracts, can cause irreversible blindness or significant loss of vision. Measuring the intraocular pressure (IOP) is important for clinical treatment of glaucoma. Commercial tonometers use indirect methods that cannot precisely measure the IOP continuously. Continuous monitoring of the IOP is important for proper treatment of the disease [60, 62, 101–104]. In addition, the IOP can be affected by a variety of factors, such as seasonal factors, nutritional factors, and the position of the body, but more research needs to be done to understand the correlation between these factors and the IOP. Therefore, an implantable precise tonometer is required for accurate and continuous IOP measurement.

❖ Inorganic material-based intracranial pressure sensors

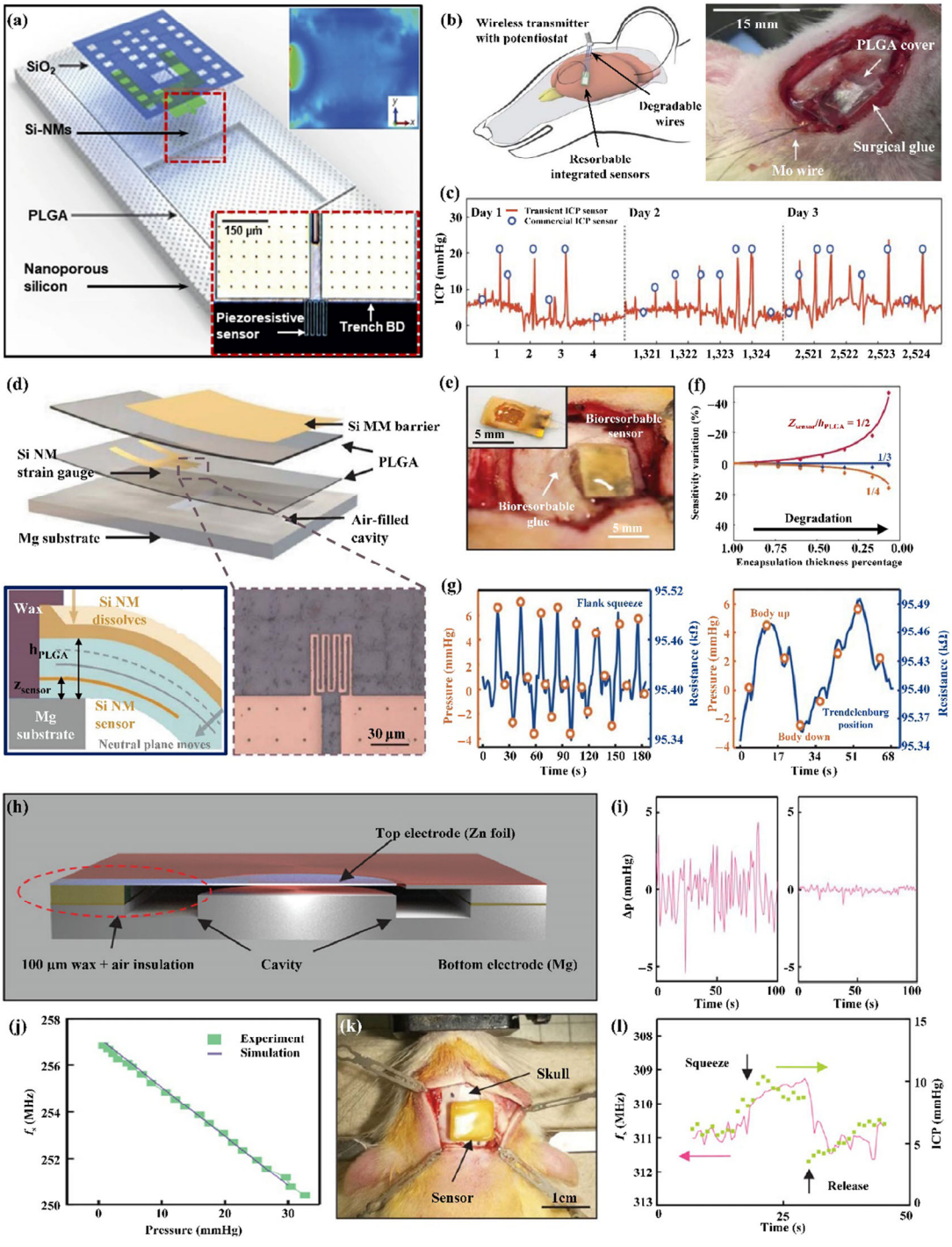

Figure 3 Inorganic material-based intracranial pressure sensors. (a) A schematic of a biodegradable (transient) pressure sensor for intracranial pressure monitoring. Top inset shows the distribution of strain in the PLGA layer from FEA when 50 mmHg external pressure is applied to the pressure sensor. Bottom inset shows an optical microscope image of the strain gauge on a trench structure. (b) An illustration and an image of the biodegradable ICP sensor inserted into the brain of a rat. (c) The monitored ICP for transient ICP sensor (red line) and commercial ICP sensor (blue dot) for 3 days. Reproduced with permission from Ref. [61], © Macmillan Publishers Limited 2016. (d) A schematic of the biodegradable pressure sensor that maintains a constant sensitivity. The natural wax which seals the edge of the device functions as the biofluid barriers as well as SiNM. Bottom left inset shows the shift of the neutral mechanical plane due to the dissolution of the SiMM barrier. Bottom right inset shows an optical microscope image of the strain gauge on an air-filled cavity. (e) An image of the implanted biodegradable ICP sensor on the brain, where the sensor was sealed with commercial biodegradable glue. (f) The sensitivity variation of the pressure sensor with different ratios of the height of SiNM in PLGA to the thickness of the encapsulation layer while the degradation process of the top encapsulation layer occurs. (g) *In vivo* results of the biodegradable ICP sensor (blue line) and commercial ICP sensor (orange dot). Reproduced with permission from Ref. [62], © WILEY-VCH Verlag GmbH & Co. KGaA, Weinheim 2020. (h) A schematic of wireless bioresorbable monitoring of the pressure by sensing the resonant frequency change. The sensing part (top electrode) of the sensor is placed on a burr hole to monitor the intracranial pressure. (i) ICP fluctuation of the wireless bioresorbable pressure sensor without wax and air encapsulation (left) and with wax and air encapsulation (right). (j) The resonant frequency change according to the pressure for the fabricated bioresorbable pressure sensor (green) and simulation result (purple). (k) An image of implanted bioresorbable pressure sensor inserted between the skull and dermis of a rat. (l) The results of the bioresorbable pressure sensor (pink line) and commercial ICP sensor (green dot) when the flanks of the rat had been squeezed. Reproduced with permission from Ref. [63], © Wiley-VCH GmbH 2020.

Recently, a microscale implantable IOP sensor with a sensitivity of 0.29 mmHg in the range of 0–40 mmHg has been fabricated [102]. The device has a disk-shaped silicon-based microchamber that serves as a pressure-sensitive air cavity. A cylindrical bottom mirror is placed in the center of the microchamber for reflection (Fig. 4(a)). A deformable silicon nitride (SiN) membrane with a gold nanodot array is fabricated on the microchamber with a distance of 7 μm between the

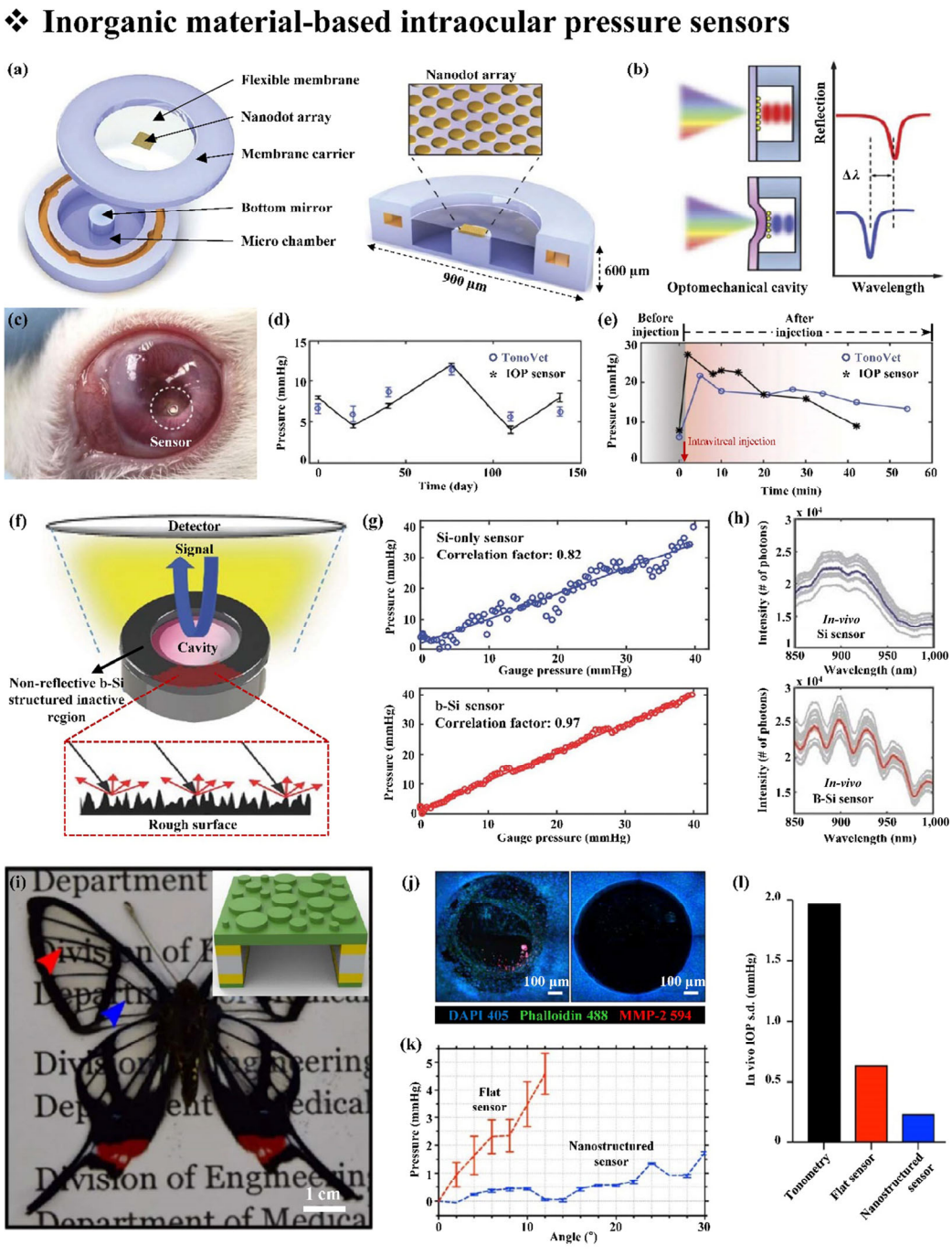

Figure 4 Inorganic material-based intraocular pressure sensors. (a) A schematic of an intraocular pressure sensor with a nanodot patterned SiN membrane to sense the pressure more efficiently. The bottom structure is composed of a Si-based bottom mirror and an air-filled cavity. (b) The wavelength of the reflected light changes while pressure is applied. (c) An image of the nanodot array IOP sensor implanted in a rabbit eye for an *in vivo* test. (d) and (e) The results of intraocular pressure changes after 138 days implantation and acute intraocular pressure change after injecting hypertonic silane after 138 days of implantation. The blue circle indicates the commercial IOP sensor (TonoVet), and the black star indicates the nanodot-patterned IOP sensor. Reproduced with permission from Ref. [102], © Lee, J. O. et al. 2017. (f) A schematic of an intraocular pressure sensor with b-Si on the edge of the device. (g) IOP measurement of b-Si (bottom graph; red line) and Si-only sensor(top graph; blue line). (h) The Si-only sensor and b-Si sensor result under slit-lamp illumination. Reproduced with permission from Ref. [103], © WILEY-VCH Verlag GmbH & Co. KGaA, Weinheim 2017. (i) An image of the postdiscal (red arrow) and basal (blue arrow) areas of the C. *faunus* butterfly. The structure of the IOP sensor has a nanopatterned Si_3N_4 layer and an air cavity structure (top inset). (j) An immunofluorescence confocal microscopy image of the flat Si_3N_4 sensor and nanostructured Si_3N_4 sensor after one month of the *in vivo* test. Compared to the flat Si_3N_4 sensor, the nanostructured Si_3N_4 sensor has almost no immune response due to foreign body reaction. The markers DAPI (blue), phalloidin (green) and MMP-2 (red) represent the cell nucleus marker, cell F-actin marker and matrix metalloproteinase marker, respectively. (k) The result of pressure to different angle for flat sensor and nanostructured sensor. (l) The standard deviation of the *in vivo* measured IOP for the conventional tonometer and flat and nanostructured IOP sensors. Reproduced with permission from Ref. [104], © Macmillan Publishers Limited, part of Springer Nature 2018.

membrane and bottom mirror. When pressure is applied, the wavelength of the reflected light changes due to the deformation of the nanodot array on the flexible membrane (Fig. 4(b)). The fabricated implantable IOP sensor has been mounted on the well-established intraocular lens (IOL) and inserted into a rabbit's eye (Fig. 4(c)). Compared to the commercial tonometer, the fabricated implantable IOP sensor shows similar sensitivity for 138 days (Fig. 4(d)).

Additionally, by intravitreal injection of hypertonic saline, instant changes in the IOP have been monitored successfully with the fabricated IOP sensor (Fig. 4(e)) [103]. However, since the edge of the sensor is fabricated with the same material as the bottom mirror (silicon), noise can be caused by reflection from the silicon edge. To reduce the noise, researchers changed the surface of the edge of the device to black-silicon (b-Si) by using a reactive ion etching (RIE) process (Fig. 4(f)). The non-reflective rough surface of b-Si reduces the noise with a correlation factor of 0.97, while the Si-only sensor has a correlation factor of 0.82. By applying the b-Si to the edge of the sensor, not only the precision of the device but also the readout distance and antibiofouling effects significantly increase. The root-mean-square error (RMSE) and peak-to-peak fluctuation are 1.96 and ±8 mmHg for the Si-only sensor and 0.58 mmHg and less than ±2 mmHg for the b-Si sensor, respectively, which indicates improved sensitivity (Figs. 4(g) and 4(h)). Since the clinically allowed peak-to-peak fluctuation is ±2 mmHg, the b-Si sensor is an improvement to the commercial tonometer.

The wings of the longtail glass wing butterfly (*Chorinea faunus*) existing in nature have another function as well as a flying function. *Chorinea faunus (C. faunus)* has a nanostructure on its surface with an aspect ratio of 1. By having nanostructured features, the wing is highly transparent and anti-reflective and simultaneously has an anti-biofouling characteristic by preventing cellular growth. By applying nanostructures with a low aspect ratio (< 1) to a freestanding Si_3N_4 membrane, an antireflective and anti-biofouling implantable IOP sensor has been fabricated (Fig. 4(i)) [104]. Cell adhesion and an inflammatory response do not occur on the nanostructured Si_3N_4 membrane (Fig. 4(j)). In addition, the sensed pressure drifts according to the increment of the angle for the flat surfaced sensor, while a slight pressure shift occurs for the nanostructured surface sensor that is negligible (Fig. 4(k)). According to these characteristics, the standard deviation (s.d.) is 0.23 mmHg for the nanostructured sensor, while it is 1.97 and 0.64 mmHg for tonometers and the flat surfaced sensor, respectively (Fig. 4(l)).

3 Carbon-based pressure sensors

Carbon-based materials, such as graphene (including graphene oxide (GO), reduced graphene oxide (rGO), graphite, carbon black, and carbon nanotubes (CNTs)), have great potential in various fields due to their good electrical conductivity, and they usually have higher mechanical and chemical stability with lighter weight compared to metals [105–112]. They are utilized in many fields, such as wearable and flexible sensors, due to their superior properties. In particular, strain/pressure sensors for wide biomedical applications are fabricated with very simple, cost-effective methods such as those involving drawing pencils [113, 114]. Because each carbon material has its own unique characteristics and can have various morphologies, we can choose suitable carbon allotropes for each application that satisfy the physical and electrical properties. In this section, we introduce examples of carbon-based pressure sensors by reviewing the performance and structure of the devices.

3.1 Carbon-based wearable pressure sensors

Carbon-based materials are promising materials for wearable and flexible sensors that can be used for detecting external pressure or sensing electrophysiological signals. In comparison with other candidate materials, advanced carbon materials have combined superiorities in designing wearable pressure sensors in the form of fibers, foam, or film due to their good electrical conductivity and excellent thermal and long-term stability, which can facilitate functionalization with other materials. Various carbon materials, including CNTs, graphene, carbon black powder, and carbon nanofibers, can be used for designing high-performance piezoresistive and piezocapacitive pressure sensors as well as piezoelectric and triboelectric sensors with microengineering of the structure and material morphology [115–118]. To date, they have been utilized as sensitive conducting layers owing to their excellent mechanical properties and good electrical characteristics. But there are some challenges to prevent undesirable toxicity of carbon-based material for stable operation as a pressure sensor. So it is important to minimize toxicity by encapsulating device with biocompatible materials.

Pressure sensors use modified sensing materials that exhibit altered electrical characteristics in response to external stimuli. The deformation of the material or modified contact area of the elements leads to changes in the electrical properties, including the resistance and capacitance. This mechanism transduces mechanical stimuli into electrical signals, enabling the detection of external pressure. Thus, flexible pressure sensors as electronic skin platforms allow sensing of external tactile pressure as well as detection of physiological signals for monitoring body activity. Here, we mainly introduce the applications of wearable pressure sensors with advanced carbon materials. The characteristics and performances of the carbon-based wearable pressure sensors are compared in the Table 3.

3.1.1 *Carbon-based tactile sensors*

For human-machine interfacing, tactile sensing is of great interest for wearable and portable electronics such as electronic skin and smart robotics. The key components for tactile sensing are high sensitivity to changes in force amplitude and direction, fast response time, flexibility and mechanical stability [119]. Advanced carbon materials and modified structures can provide enhanced sensitivity, which enables grabbing of objects and detection of surface texture, contact location and direction of external stimuli, which cannot be easily obtained with traditional methods. To obtain these parameters, mimicking

Table 3 The characteristics and performances of the carbon-based wearable pressure sensors

Material	Type	Pressure range	Sensitivity	Response time	Reference
3D hill structure of CNT/PU	Piezocapacitive	< 1 kPa/600 kPa	0.26 kPa^{-1}/0.04 kPa^{-1}	ms range	[120]
CNT TFTs	Piezoresistive	< 6.8 kPa	—	< 30 ms	[121]
Ni-coated textile/CNT-coated cotton	Piezoresistive	< 15 kPa	14.4 kPa^{-1}	24 ms	[124]
rGO aerogel/rGO paper	Piezoresistive	< 0.72 Pa/130 kPa	300 kPa^{-1}	8 ms	[125]
Laser-induced graphene	Piezoresistive	< 100 Pa/1 kPa	480 kPa^{-1}/0.9 kPa^{-1}	2 μs	[127]
Biomimetic CNT/PDMS composite	Piezoresistive	< 140 Pa/10 kPa	83.9 kPa^{-1}/0.4 kPa^{-1}	~ 170 ms	[128]

biological functions and structure can be a prominent method that can be applied to both resistance- and capacitance-type modes. As shown in Figs. 5(a)–5(c), the electronic skin mimics key sensory structures: protrusion of the inner surface and mechanoreceptors in the spinosum that enable amplification of tactile signals caused by normal and shear stress [120]. It is designed with an array of capacitors that include CNTs as top and bottom electrodes and PU elastomer as a substrate that can deform elastically to external pressure. The key aspect of this device is that it can distinguish not only the pressure strength but also the pressure direction. The three-dimensional (3D) geometric design of e-skin involves different deformations of the layer according to the direction of the external force; the capacitance of the side exposed to greater pressure has a larger increase than that of the side opposite to the applied pressure. Figure 5(d) illustrates the response characteristics of biomimetic skin, which enables differentiation of the shear stress by comparing the results from different pixels.

Building a large-area flexible sensor with high resolution is key to designing practical pressure sensors. By fabricating the pixels in active mode over a 4 inch area with CNTs, high uniformity and excellent sensing accuracy with low operating power (3 V) can be obtained [121]. The whole sensor is made of an active matrix of a 16 × 16 CNT thin film transistor, which offers high performance due to its large current density, high mobility and fast response time (< 30 ms), as depicted in Fig. 5(e). Figure 5(f) shows microscope image of individual CNT thin film transistor. The high flexibility and robustness to a large bending radius enable uniform performance not only on a flat surface but also on a curved surface, showing similar results. A CNT thin film is used in the channel with high density, which has a typical length of 1 μm, as illustrated in

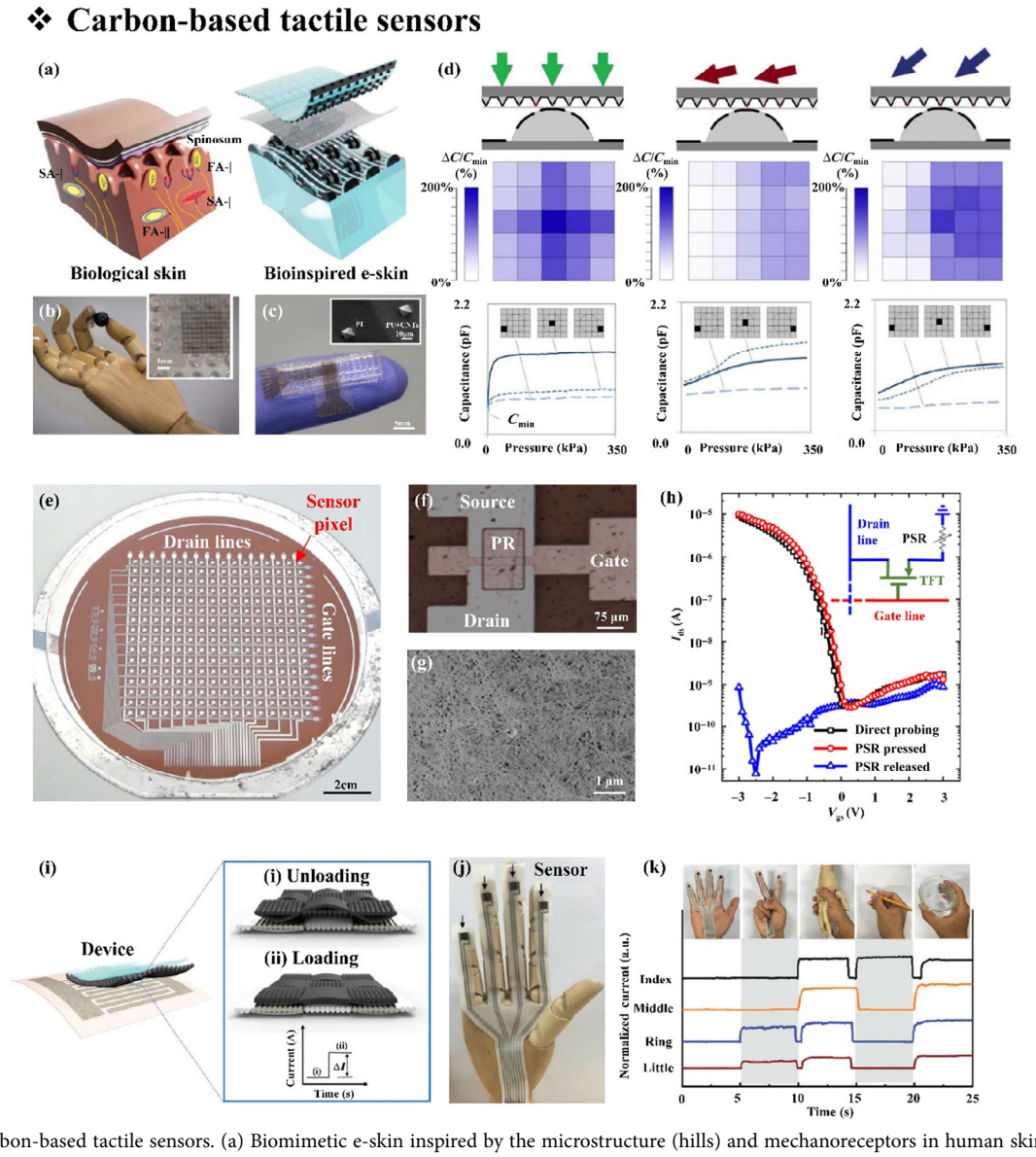

Figure 5 Carbon-based tactile sensors. (a) Biomimetic e-skin inspired by the microstructure (hills) and mechanoreceptors in human skin. Black, CNT electrodes; blue, PU elastomer; gray, intermediate layer. (b) Optical image of fabricated e-skin and inset shows closer view of the hill structure. (c) CNT-PU interconnects for signal recording and inset shows SEM image of the top layer. (d) Functionality of designed e-skin based on multiple pixels for applied shear stress; sensor array with 5 by 5 capacitors with a relative change. Dashed circles indicate the locations of sensors. Reproduced with permission from Ref. [120], © Boutry, C. M. et al. 2018. (e) Optical image of a 16 by 16 carbon nanotube thin film transistor. (f) Microscopic image of a CNT TFT. Photoresist (PR) defines the channel. (g) SEM image of deposited high-density CNT thin film. (h) Transfer curve (V_{gs}–I_{ds}) when V_{ds} = −1 V in pressed mode and released mode. The inset shows the circuit diagram for a single pixel. Reproduced with permission from Ref. [121], © American Chemical Society 2018. (i) Schematic illustration of a textile pressure sensor. (j) Optical image of the textile sensor covering an artificial hand. (k) Current signal detection according to different hand motions for each finger. Reproduced with permission from Ref. [124], © WILEY-VCH Verlag GmbH & Co. KGaA, Weinheim 2017.

Fig. 5(g). Figure 5(h) shows the transfer curve and the overall design of the pressure sensor, which indicates that the pressure-sensitive rubber (PSR) is grounded and connected to the source of the CNT TFT and that the gate and drain are biased separately. Integrating CNTs in high performance pressure sensor with flexibility and stretchability would contribute to practical electronic skin.

Wearable pressure sensors are usually combined with other materials that have low modulus and softness for conformal contact with the skin and high sensitivity. The typical method for fabricating low modulus composites is to use carbon/polymer composites that are cost-effective and have potential for application in wearable health monitoring and soft robotics [122, 123]. Except for when utilizing polymers, a textile pressure sensor is fabricated on common fabric [124]. As illustrated in Fig. 5(i), an interdigitated electrode is fabricated on a commercial polyester textile by laser scribing followed by deposition of conformal Ni. A piece of cotton dip coated with CNTs is assembled with the interdigitated electrodes. Applying external pressure increases the contact area between the nanostructure of the Ni textile and CNT fabric, which results in a current increase due to more pathways between these films. A textile pressure sensor can be attached to curved skin to detect the gesture of each finger, where the current increases with the bending angle of each finger, as illustrated in Figs. 5(j) and 5(k).

3.1.2 *Carbon-based physiological signal sensors*

Recently, there has been an increasing demand for flexible, wearable pressure sensors that can monitor physiological signals for personal healthcare systems. Carbon-based materials have great potential for application in healthcare systems because they have high performance, low cost and ease of functionalization. An all-carbon pressure sensor with rGO nanomaterials demonstrates ultrahigh sensitivity (349–253 kPa^{-1}) in the low pressure regime and low energy consumption (~ 0.58 μW) with a fast response time (8 ms at 1 kPa) [125]. As shown in Figs. 6(a) and 6(b), an rGO aerogel which has a good elasticity is sandwiched between the two pieces of flexible rGO paper performing the role as an electrode material. A 3D surface height map (Fig. 6(c)) demonstrates that lots of rGO sheet ends make rGO aerogel has a rough surface that contacts with the relatively flat surfaces of the rGO electrodes. When external pressure is applied, the rough surface of the rGO aerogel deforms, which leads to a decrease in electrical resistance due to the enlarged contact area. Owing to its high sensitivity and fast response, the all-carbon pressure sensor can detect weak pulse waves on wrists. The real-time recorded electrical signal can distinguish the modes of the pulse waveform, indicating incident blood flow (P1) and two reflected blood flows from the hand (P2) and lower body (P3), as illustrated in Figs. 6(d) and 6(e). Figure 6(f) shows the high stability and recoverability through a loading-unloading cycle test.

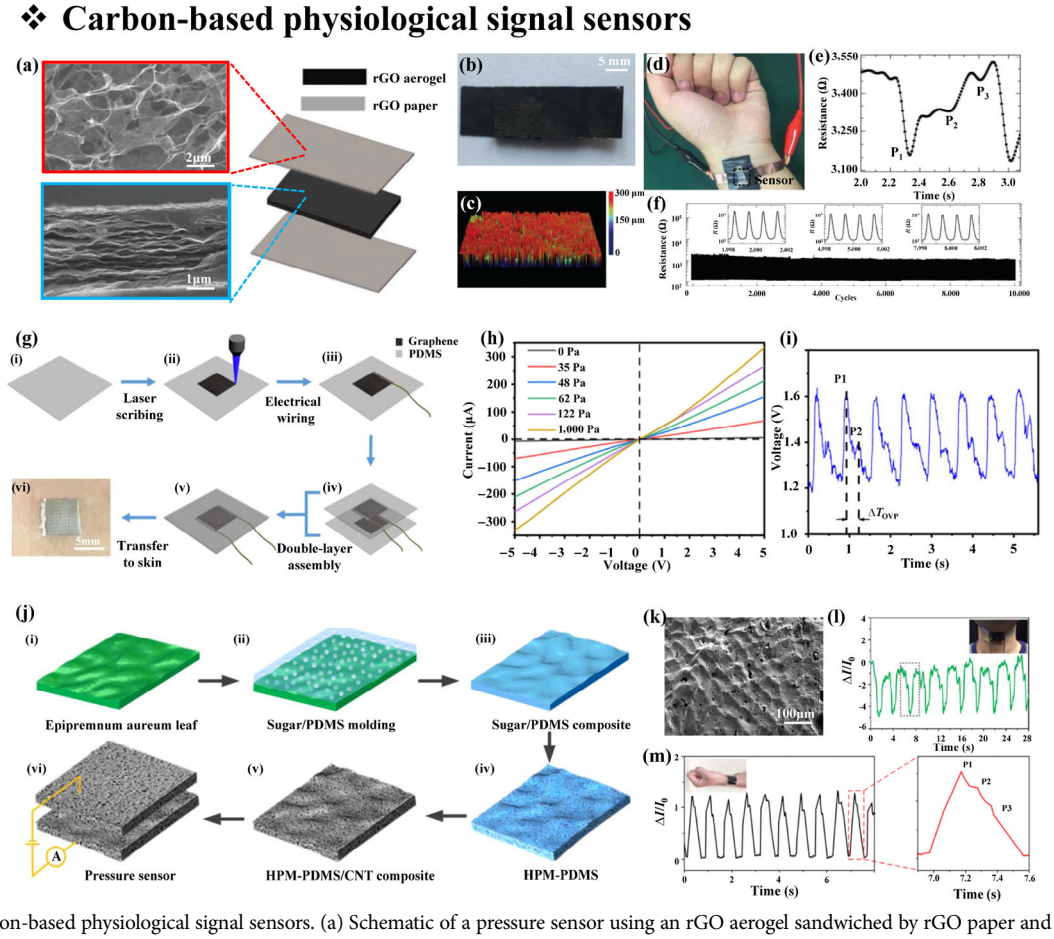

Figure 6 Carbon-based physiological signal sensors. (a) Schematic of a pressure sensor using an rGO aerogel sandwiched by rGO paper and SEM images of rGO aerogel surface and cross-section of an rGO paper. (b) Optical image of the carbon-based pressure sensor. (c) 3D image of the rGO aerogel surface height. (d) Optical image of sensing the arterial pulse wave. (e) Resistance signal of a single waveform for detecting the arterial pulse. (f) Cycling test for checking the stability of the sensor. Inset shows the magnified three curves. Reproduced with permission from Ref. [125], © WILEY-VCH Verlag GmbH & Co. KGaA, Weinheim 2019. (g) Fabrication method of a laser-induced graphene pressure sensor. (h) *I*–*V* curve under various pressures. (i) Recorded electrical signal of the pressure sensor for detecting sphygmus. Reproduced with permission from Ref. [127], © American Chemical Society 2019. (j) Fabrication process of a hybrid porous microstructure pressure sensor. (k) SEM image of the hybrid porous PDMS/carbon nanotube composite. (l) Recorded electrical signal for detecting the arterial pulse. (m) Real-time recording for detecting swallowing activity. Reproduced with permission from Ref. [128], © American Chemical Society 2019.

Low-cost, simple fabrication of pressure sensors is important for practically sensing human physiological signals. One of the simple methods for making graphene is to directly stimulate carbon materials with a laser in ambient atmosphere [126]. As shown in Fig. 6(g), an epidermal pressure sensor is fabricated with a simple and low-cost approach by making laser-induced graphene from PDMS, which shows high electrical conductivity and mechanical stability [127]. Two pieces of conductive graphene layer that have porous-like features are assembled together and transferred to the skin. Figure 6(h) shows the linear characteristics of the *I*–*V* curves under different pressures and an obvious increase in conductance with external stimuli. After attaching a laser-induced graphene pressure sensor to the skin, it distinguishes the heartbeat by monitoring pulse waves, as depicted in Fig. 6(i).

Mimicking bionic microstructures can contribute to realizing high-sensitivity pressure sensors by copying their surface or structure characteristics. Figure 6(j) shows a bioinspired, sensitive, piezoresistive pressure sensor based on a hybrid porous microstructure fabricated by using a leaf and sugar as a template that makes the elastic modulus of the sensor low and forms a porous structure in PDMS, followed by immersion in a multiwalled CNT water solution [128]. The hybrid porous microstructure PDMS (Fig. 6(k)) shows a 83.9 kPa^{-1} sensitivity at low pressure due to its porous structure and increase in contact area and conductive pathway. Figures 6(l) and 6(m) show potential applications with this hybrid porous microstructure for detecting physiological signals, including wrist pulse, swallowing activity, finger movement, or vibration.

3.2 Carbon-based implantable pressure sensors

For application to an organ that expands up to 100%, such as the bladder, materials that can measure extreme strain should be considered. Carbon-based materials, such as carbon black and CNTs, are candidate materials that can be applied to bladder pressure monitoring sensors. Doping carbon materials into silicone elastomers, such as PDMS or EcoFlex, increases the sheet resistance by several orders of magnitude compared to conductive PDMS with metallic nanoparticles. This increased sheet resistance enhances the piezoresistive effect of the carbon-doped silicone.

The bladder pressure can be measured by sensing the volume change of the bladder, which is the size change during extraction and contraction. Figures 7(a) and 7(b) show bladder

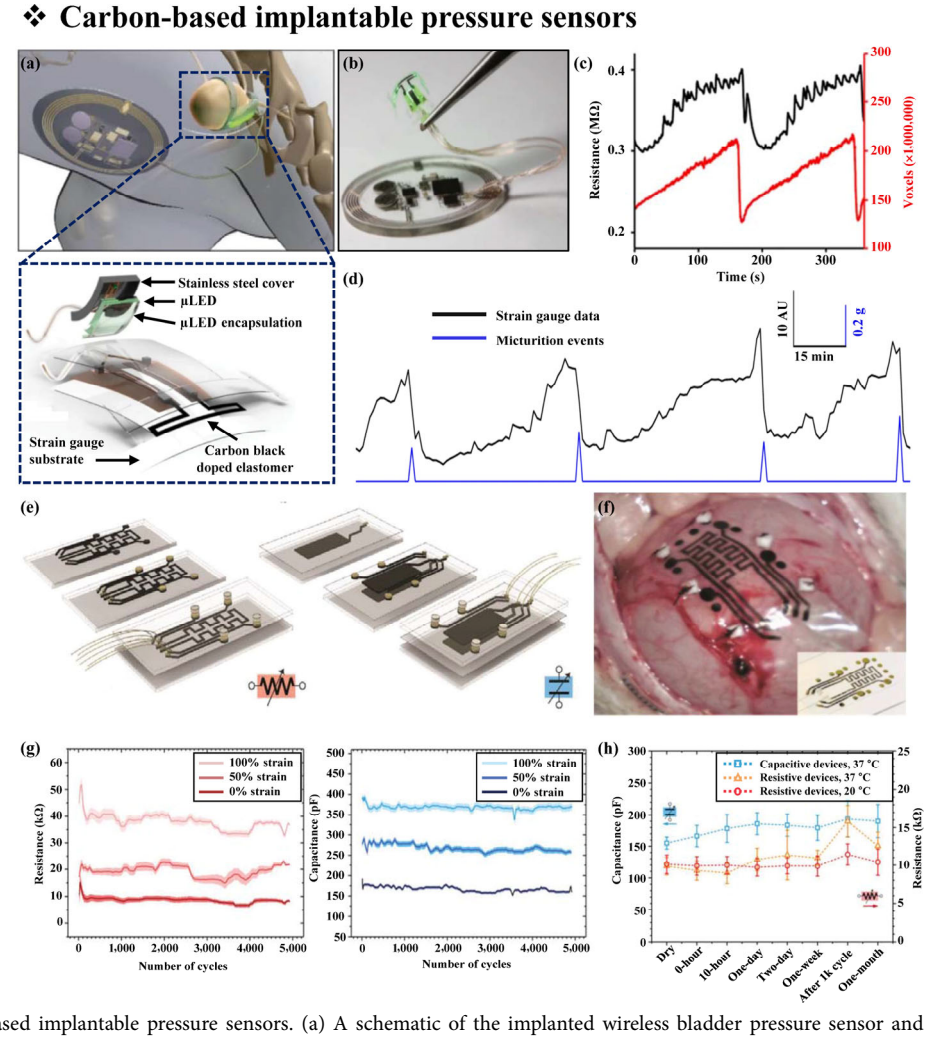

Figure 7 Carbon-based implantable pressure sensors. (a) A schematic of the implanted wireless bladder pressure sensor and optogenetic peripheral neuromodulation device. The carbon black-doped pressure sensor embedded in the EcoFlex substrate, which is stretchable, and the μLED module for optoelectronic stimulation. (b) A illustration of the wireless power supply module. (c) The resistance change of bladder pressure sensor (black) and the bladder size change (red) during extraction and contraction of the bladder. (d) The bladder pressure change obtained from the implanted bladder pressure sensor in the freely moving state during micturition events. Reproduced with permission from Ref. [129], © Springer Nature Limited 2019. (e) A schematic of the single-wall CNT-doped piezoresistive pressure sensor and piezocapacitive pressure sensor. (f) An image of the pressure sensor implanted on the bladder to monitor the bladder pressure. (g) The 5,000-cycle strain test results of piezoresistive pressure sensor (red line) and piezocapacitive pressure sensor (blue line). (h) The stability of the two types of pressure sensors under physiological conditions (PBS solution at 37 °C). Reproduced with permission from Ref. [130], © WILEY-VCH Verlag GmbH & Co. KGaA, Weinheim 2019.

pressure monitoring by wrapping the pressure sensor around the bladder and applying optical stimulation, known as optogenetics, to control voiding [129]. When abnormal bladder pressure is measured, the Bluetooth system operates the micro light-emitting diode (μLED) of the optoelectronic stimulation and sensing (OESS) module to activate the opsin, which can only stimulate a specific type of cell. By measuring the expansion and contraction of the bladder, the voiding status can be distinguished. The bladder pressure sensor which encircles the bladder is fabricated with carbon black-doped silicone (EcoFlex). To secure the biocompatibility, the sensor is encapsulated with PDMS/polyisobutylene. The deformation of the bladder due to encircling of the bladder with the sensor does not exceed 2%, which is negligible. The resistance of bladder pressure changes by respect to the change in bladder size which indicates the fabricated pressure sensor can monitor the bladder activity precisely (Fig. 7(c)). Figure 7(d) shows the bladder pressure monitored under acute stimulation of the bladder in a micturition cage, and the resistance of the strain gauge decreases rapidly, which indicates bladder contraction.

Figure 7(e) shows the bladder pressure monitoring and stimulation device using single wall CNTs [130]. Two types of devices have been fabricated: piezoresistive and piezocapacitive. For the piezoresistive sensor, the bladder pressure is measured based on the resistance changes due to changes in the number of conductive pathways in the CNT network. For the piezocapacitive pressure sensor, the capacitance changes with the area increment of the double layered CNTs and thickness decrement of the dielectric layer during bladder expansion. Figure 7(g) shows the piezoresistive pressure sensor fluctuate more than piezocapacitive pressure sensor during 5,000 cycle tests. Since implantable devices are implanted into the body, maintaining stable performance in a physiological environment is important. Figure 7(h) shows the stable performance with little fluctuation of the fabricated pressure sensors when soaked in saline solution for up to one month. The piezoresistive pressure sensor shows more fluctuation compare to the piezocapacitive pressure sensor after a 1,000-cycle test and one week of immersion. However, the piezoresistive pressure sensor has a relatively simple circuit design, while the piezocapacitive pressure sensor has a complicated circuit and is affected by the parasitic capacitance of the nearby tissues. Therefore, both the resistance- and capacitance-based pressure sensors have pros and cons. Additionally, future studies are required to ensure the biocompatibility of the sensors and provide chronic *in vivo* validation.

4 Conclusion

As many industries, including robotics and the medical field, develop, the demand for more specialized and high-performance pressure sensors increases. This review covered some of the most recent advances in high-performance wearable and implantable pressure sensors based on inorganic materials, metals and carbon. As highlighted in this review, by combining novel inorganic materials, metals and carbon-based materials with unique structures, the performance of flexible pressure sensors has been significantly improved compared to that of conventional pressure sensors, which can establish an innovative foundation for bioelectronics. In addition, the sensing performance can be significantly improved by enhancing the adhesion between the sensor and the surface of the target, which is another challenge to be solved. Furthermore, flexible pressure sensors can pave the way for the human healthcare sector via cooperation among various rapidly developing research fields such as electronic engineering, biomedical engineering, material science, and tissue engineering.

Acknowledgements

This work acknowledges the support received from the National Research Foundation of Korea (Nos. NRF-2018M3A7B4071109 and NRF-2019R1A2C2086085).

References

[1] Chen, L. Y.; Tee, B. C. K.; Chortos, A. L.; Schwartz, G.; Tse, V.; Lipomi, D. J.; Wong, H. S. P.; McConnell, M. V.; Bao, Z. N. Continuous wireless pressure monitoring and mapping with ultra-small passive sensors for health monitoring and critical care. *Nat. Commun.* **2014**, *5*, 5028.

[2] Chu, M.; Nguyen, T.; Pandey, V.; Zhou, Y. X.; Pham, H. N.; Bar-Yoseph, R.; Radom-Aizik, S.; Jain, R.; Cooper, D. M.; Khine, M. J. N. Respiration rate and volume measurements using wearable strain sensors. *npj Digital Med.* **2019**, *2*, 8.

[3] Guo, Y.; Zhong, M. J.; Fang, Z. W.; Wan, P. B.; Yu, G. H. A wearable transient pressure sensor made with MXene nanosheets for sensitive broad-range human–machine interfacing. *Nano Lett.* **2019**, *19*, 1143–1150.

[4] Luo, N. Q.; Dai, W. X.; Li, C. L.; Zhou, Z. Q.; Lu, L. Y.; Poon, C. C. Y.; Chen, S. C.; Zhang, Y. T.; Zhao, N. Flexible piezoresistive sensor patch enabling ultralow power cuffless blood pressure measurement. *Adv. Funct. Mater.* **2016**, *26*, 1178–1187.

[5] Pang, Y.; Zhang, K. N.; Yang, Z.; Jiang, S.; Ju, Z. Y.; Li, Y. X.; Wang, X. F.; Wang, D. Y.; Jian, M. Q.; Zhang, Y. Y. et al. Epidermis microstructure inspired graphene pressure sensor with random distributed spinosum for high sensitivity and large linearity. *ACS Nano* **2018**, *12*, 2346–2354.

[6] Boutry, C. M.; Kaizawa, Y.; Schroeder, B. C.; Chortos, A.; Legrand, A.; Wang, Z.; Chang, J.; Fox, P.; Bao, Z. N. A stretchable and biodegradable strain and pressure sensor for orthopaedic application. *Nat. Electron.* **2018**, *1*, 314–321.

[7] Huang, W. J.; Dai, K.; Zhai, Y.; Liu, H.; Zhan, P. F.; Gao, J. C.; Zheng, G. Q.; Liu, C. T.; Shen, C. Y. Flexible and lightweight pressure sensor based on carbon nanotube/thermoplastic polyurethane-aligned conductive foam with superior compressibility and stability. *ACS Appl. Mater. Interfaces* **2017**, *9*, 42266–42277.

[8] Jeong, Y.; Park, J.; Lee, J.; Kim, K.; Park, I. Ultrathin, biocompatible, and flexible pressure sensor with a wide pressure range and its biomedical application. *ACS Sens.* **2020**, *5*, 481–489.

[9] Nathan, A.; Ahnood, A.; Cole, M. T.; Lee, S.; Suzuki, Y.; Hiralal, P.; Bonaccorso, F.; Hasan, T.; Garcia-Gancedo, L.; Dyadyusha, A. et al. Flexible electronics: The next ubiquitous platform. *Proc. IEEE* **2012**, *100*, 1486–1517.

[10] Sun, Y.; Rogers, J. A. Inorganic semiconductors for flexible electronics. *Adv. Mater.* **2007**, *19*, 1897–1916.

[11] MacDonald, W. A.; Looney, M. K.; MacKerron, D.; Eveson, R.; Adam, R.; Hashimoto, K.; Rakos, K. Latest advances in substrates for flexible electronics. *J. Soc. Inf. Dis.* **2007**, *15*, 1075–1083.

[12] Song, K. I.; Seo, H.; Seong, D.; Kim, S.; Yu, K. J.; Kim, Y. C.; Kim, J.; Kwon, S. J.; Han, H. S.; Youn, I. et al. Adaptive self-healing electronic epineurium for chronic bidirectional neural interfaces. *Nat. Commun.* **2020**, *11*, 4195.

[13] Chiang, C. H.; Won, S. M.; Orsborn, A. L.; Yu, K. J.; Trumpis, M.; Bent, B.; Wang, C.; Xue, Y. G.; Min, S.; Woods, V. et al. Development of a neural interface for high-definition, long-term recording in rodents and nonhuman primates. *Sci. Transl. Med.* **2020**, *12*, eaay4682.

[14] Mishra, S.; Kim, Y. S.; Intarasirisawat, J.; Kwon, Y. T.; Lee, Y.; Mahmood, M.; Lim, H. R.; Herbert, R.; Yu, K. J.; Ang, C. S. et al. Soft, wireless periocular wearable electronics for real-time detection of eye vergence in a virtual reality toward mobile eye therapies. *Sci. Adv.* **2020**, *6*, eaay1729.

[15] Song, E. M.; Chiang, C. H.; Li, R.; Jin, X.; Zhao, J. N.; Hill, M.; Xia, Y.; Li, L. Z.; Huang, Y. M.; Won, S. M. et al. Flexible electronic/optoelectronic microsystems with scalable designs for chronic biointegration. *Proc. Natl. Acad. Sci. USA* **2019**, *116*, 15398–15406.

[16] Chun, S.; Kim, D. W.; Kim, J.; Pang, C. A transparent, glue-free, skin-attachable graphene pressure sensor with micropillars for skin-elasticity measurement. *Nanotechnology* **2019**, *30*, 335501.
[17] Kang, S.; Cho, S.; Shanker, R.; Lee, H.; Park, J.; Um, D. S.; Lee, Y.; Ko, H. Transparent and conductive nanomembranes with orthogonal silver nanowire arrays for skin-attachable loudspeakers and microphones. *Sci. Adv.* **2018**, *4*, eaas8772.
[18] Song, E. M.; Li, R.; Jin, X.; Du, H. N.; Huang, Y. M.; Zhang, J. Z.; Xia, Y.; Fang, H.; Lee, Y. K.; Yu, K. J. et al. Ultrathin trilayer assemblies as long-lived barriers against water and ion penetration in flexible bioelectronic systems. *ACS Nano* **2018**, *12*, 10317–10326.
[19] Yu, K. J.; Yan, Z.; Han, M. D.; Rogers, J. A. Inorganic semiconducting materials for flexible and stretchable electronics. *npj Flex. Electron.* **2017**, *1*, 4.
[20] Kim, S.; Amjadi, M.; Lee, T. I.; Jeong, Y.; Kwon, D.; Kim, M. S.; Kim, K.; Kim, T. S.; Oh, Y. S.; Park, I. Wearable, ultrawide-range, and bending-insensitive pressure sensor based on carbon nanotube network-coated porous elastomer sponges for human interface and healthcare devices. *ACS Appl. Mater. Interfaces* **2019**, *11*, 23639–23648.
[21] Duan, X. F.; Huang, Y.; Agarwal, R.; Lieber, C. M. Single-nanowire electrically driven lasers. *Nature* **2003**, *421*, 241–245.
[22] Hyun, J. K.; Zhang, S. X.; Lauhon, L. J. Nanowire heterostructures. *Ann. Rev. Mater. Res.* **2013**, *43*, 451–479.
[23] Cohen-Karni, T.; Lieber, C. M. Nanowire nanoelectronics: Building interfaces with tissue and cells at the natural scale of biology. *Pure Appl. Chem.* **2013**, *85*, 883–901.
[24] Koh, W. K.; Saudari, S. R.; Fafarman, A. T.; Kagan, C. R.; Murray, C. B. Thiocyanate-capped PbS nanocubes: Ambipolar transport enables quantum dot based circuits on a flexible substrate. *Nano Lett.* **2011**, *11*, 4764–4767.
[25] Son, J. S.; Lee, J. S.; Shevchenko, E. V.; Talapin, D. V. Magnet-in-the-semiconductor nanomaterials: High electron mobility in all-inorganic arrays of FePt/CdSe and FePt/CdS core–shell heterostructures. *J. Phys. Chem. Lett.* **2013**, *4*, 1918–1923.
[26] Rogers, J. A.; Lagally, M. G.; Nuzzo, R. G. Synthesis, assembly and applications of semiconductor nanomembranes. *Nature* **2011**, *477*, 45–53.
[27] Fang, H.; Zhao, J. N.; Yu, K. J.; Song, E. M.; Farimani, A. B.; Chiang, C. H.; Jin, X.; Xue, Y. G.; Xu, D.; Du, W. B. et al. Ultrathin, transferred layers of thermally grown silicon dioxide as biofluid barriers for biointegrated flexible electronic systems. *Proc. Natl. Acad. Sci. USA* **2016**, *113*, 11682–11687.
[28] Lee, J. S.; Kovalenko, M. V.; Huang, J.; Chung, D. S.; Talapin, D. V. Band-like transport, high electron mobility and high photoconductivity in all-inorganic nanocrystal arrays. *Nat. Nanotechnol.* **2011**, *6*, 348–352.
[29] Dutta, P.; Rathi, M.; Zheng, N.; Gao, Y.; Yao, Y.; Martinez, J.; Ahrenkiel, P.; Selvamanickam, V. High mobility single-crystalline-like GaAs thin films on inexpensive flexible metal substrates by metal-organic chemical vapor deposition. *Appl. Phys. Lett.* **2014**, *105*, 092104.
[30] Viventi, J.; Kim, D. H.; Vigeland, L.; Frechette, E. S.; Blanco, J. A.; Kim, Y. S.; Avrin, A. E.; Tiruvadi, V. R.; Hwang, S. W.; Vanleer, A. C. et al. Flexible, foldable, actively multiplexed, high-density electrode array for mapping brain activity *in vivo*. *Nat. Neurosci.* **2011**, *14*, 1599–1605.
[31] Xu, L. Z.; Gutbrod, S. R.; Bonifas, A. P.; Su, Y. W.; Sulkin, M. S.; Lu, N. S.; Chung, H. J.; Jang, K. I.; Liu, Z. J.; Ying, M. et al. 3D multifunctional integumentary membranes for spatiotemporal cardiac measurements and stimulation across the entire epicardium. *Nat. Commun.* **2014**, *5*, 3329.
[32] Dagdeviren, C.; Su, Y. W.; Joe, P.; Yona, R.; Liu, Y. H.; Kim, Y. S.; Huang, Y. A.; Damadoran, A. R.; Xia, J.; Martin, L. W. et al. Conformable amplified lead zirconate titanate sensors with enhanced piezoelectric response for cutaneous pressure monitoring. *Nat. Commun.* **2014**, *5*, 4496.
[33] Park, D. Y.; Joe, D. J.; Kim, D. H.; Park, H.; Han, J. H.; Jeong, C. K.; Park, H.; Park, J. G.; Joung, B.; Lee, K. J. Self-powered real-time arterial pulse monitoring using ultrathin epidermal piezoelectric sensors. *Adv. Mater.* **2017**, *29*, 1702308.
[34] Zhu, B. W.; Ling, Y. Z.; Yap, L. W.; Yang, M. J.; Lin, F. G.; Gong, S.; Wang, Y.; An, T. C.; Zhao, Y. M.; Cheng, W. L. Hierarchically structured vertical gold nanowire array-based wearable pressure sensors for wireless health monitoring. *ACS Appl. Mater. Interfaces* **2019**, *11*, 29014–29021.
[35] Li, X.; Fan, Y. J.; Li, H. Y.; Cao, J. W.; Xiao, Y. C.; Wang, Y.; Liang, F.; Wang, H. L.; Jiang, Y.; Wang, Z. L. et al. Ultracomfortable hierarchical nanonetwork for highly sensitive pressure sensor. *ACS Nano* **2020**, *14*, 9605–9612.
[36] Trung, T. Q.; Lee, N. E. Flexible and stretchable physical sensor integrated platforms for wearable human-activity monitoringand personal healthcare. *Adv. Mater.* **2016**, *28*, 4338–4372.
[37] Xu, K. C.; Lu, Y. Y.; Takei, K. Multifunctional skin-inspired flexible sensor systems for wearable electronics. *Adv. Mater. Technol.* **2019**, *4*, 1800628.
[38] Joung, Y. H. Development of implantable medical devices: From an engineering perspective. *Int. Neurourol. J.* **2013**, *17*, 98–106.
[39] Bauer, S.; Bauer-Gogonea, S.; Graz, I.; Kaltenbrunner, M.; Keplinger, C.; Schwödiauer, R. 25th anniversary article: A soft future: From robots and sensor skin to energy harvesters. *Adv. Mater.* **2014**, *26*, 149–162.
[40] Hammock, M. L.; Chortos, A.; Tee, B. C. K.; Tok, J. B. H.; Bao, Z. A. 25th anniversary article: The evolution of electronic skin (e-skin): A brief history, design considerations, and recent progress. *Adv. Mater.* **2013**, *25*, 5997–6038.
[41] Mannsfeld, S. C. B.; Tee, B. C. K.; Stoltenberg, R. M.; Chen, C. V. H. H.; Barman, S.; Muir, B. V. O.; Sokolov, A. N.; Reese, C.; Bao, Z. A. Highly sensitive flexible pressure sensors with microstructured rubber dielectric layers. *Nat. Mater.* **2010**, *9*, 859–864.
[42] Kim, D. H.; Lu, N. S.; Ma, R.; Kim, Y. S.; Kim, R. H.; Wang, S. D.; Wu, J.; Won, S. M.; Tao, H.; Islam, A. et al. Epidermal electronics. *Science* **2011**, *333*, 838–843.
[43] Someya, T.; Sekitani, T.; Iba, S.; Kato, Y.; Kawaguchi, H.; Sakurai, T. A large-area, flexible pressure sensor matrix with organic field-effect transistors for artificial skin applications. *Proc. Natl. Acad. Sci. USA* **2004**, *101*, 9966–9970.
[44] Lam Po Tang, S. Recent developments in flexible wearable electronics for monitoring applications. *Trans. Inst. Meas. Control* **2007**, *29*, 283–300.
[45] Joo, Y.; Byun, J.; Seong, N.; Ha, J.; Kim, H.; Kim, S.; Kim, T.; Im, H.; Kim, D.; Hong, Y. Silver nanowire-embedded PDMS with a multiscale structure for a highly sensitive and robust flexible pressure sensor. *Nanoscale* **2015**, *7*, 6208–6215.
[46] Gao, L.; Zhu, C. X.; Li, L.; Zhang, C. W.; Liu, J. H.; Yu, H. D.; Huang, W. All paper-based flexible and wearable piezoresistive pressure sensor. *ACS Appl. Mater. Interfaces* **2019**, *11*, 25034–25042.
[47] Gong, S.; Schwalb, W.; Wang, Y. W.; Chen, Y.; Tang, Y.; Si, J.; Shirinzadeh, B.; Cheng, W. L. A wearable and highly sensitive pressure sensor with ultrathin gold nanowires. *Nat. Commun.* **2014**, *5*, 3132.
[48] Lee, D.; Lee, H.; Jeong, Y.; Ahn, Y.; Nam, G.; Lee, Y. Highly sensitive, transparent, and durable pressure sensors based on sea-urchin shaped metal nanoparticles. *Adv. Mater.* **2016**, *28*, 9364–9369.
[49] Xu, M. G.; Reekie, L.; Chow, Y. T.; Dakin, J. P. Optical in-fibre grating high pressure sensor. *Electron. Lett.* **1993**, *29*, 398–399.
[50] Totsu, K.; Haga, Y.; Esashi, M. Ultra-miniature fiber-optic pressure sensor using white light interferometry. *J. Micromech. Microeng.* **2005**, *15*, 71–75.
[51] Zhu, Y. Z.; Wang, A. B. Miniature fiber-optic pressure sensor. *IEEE Photonics Technol. Lett.* **2005**, *17*, 447–449.
[52] Yu, Q. X.; Zhou, X. L. Pressure sensor based on the fiber-optic extrinsic Fabry-Perot interferometer. *Photonic Sens.* **2011**, *1*, 72–83.
[53] Fang, H.; Yu, K. J.; Gloschat, C.; Yang, Z. J.; Song, E. M.; Chiang, C. H.; Zhao, J. N.; Won, S. M.; Xu, S. Y.; Trumpis, M. et al. Capacitively coupled arrays of multiplexed flexible silicon transistors for long-term cardiac electrophysiology. *Nat. Biomed. Eng.* **2017**, *1*, 0038.
[54] Song, E. M.; Fang, H.; Jin, X.; Zhao, J. N.; Jiang, C. S.; Yu, K. J.; Zhong, Y. D.; Xu, D.; Li, J. H.; Fang, G. H. et al. Thin, transferred layers of silicon dioxide and silicon nitride as water and ion barriers for implantable flexible electronic systems. *Adv. Electron. Mater.* **2017**, *3*, 1700077.
[55] Yin, M.; Borton, D. A.; Aceros, J.; Patterson, W. R.; Nurmikko, A. V.

A 100-channel hermetically sealed implantable device for chronic wireless neurosensing applications. *IEEE Trans. Biomed. Circuits Syst.* **2013**, *7*, 115–128.

[56] Bazaka, K.; Jacob, M. V. Implantable devices: Issues and challenges. *Electronics* **2013**, *2*, 1–34.

[57] Li, J. H.; Song, E. M.; Chiang, C. H.; Yu, K. J.; Koo, J.; Du, H. N.; Zhong, Y. S.; Hill, M.; Wang, C.; Zhang, J. Z. et al. Conductively coupled flexible silicon electronic systems for chronic neural electrophysiology. *Proc. Natl. Acad. Sci. USA* **2018**, *115*, E9542–E9549.

[58] Li, J. H.; Li, R.; Chiang, C. H.; Zhong, Y. S.; Shen, H. X.; Song, E. M.; Hill, M.; Won, S. M.; Yu, K. J.; Baek, J. M. et al. Ultrathin, high capacitance capping layers for silicon electronics with conductive interconnects in flexible, long-lived bioimplants. *Adv. Mater. Technol.* **2020**, *5*, 1900800.

[59] Kang, K.; Cho, Y.; Yu, K. J. Novel Nano-materials and nano-fabrication techniques for flexible electronic systems. *Micromachines* **2018**, *9*, 263.

[60] Shin, J.; Yan, Y.; Bai, W. B.; Xue, Y. G.; Gamble, P.; Tian, L. M.; Kandela, I.; Haney, C. R.; Spees, W.; Lee, Y. et al. Bioresorbable pressure sensors protected with thermally grown silicon dioxide for the monitoring of chronic diseases and healing processes. *Nat. Biomed. Eng.* **2019**, *3*, 37–46.

[61] Kang, S. K.; Murphy, R. K. J.; Hwang, S. W.; Lee, S. M.; Harburg, D. V.; Krueger, N. A.; Shin, J.; Gamble, P.; Cheng, H. Y.; Yu, S. et al. Bioresorbable silicon electronic sensors for the brain. *Nature* **2016**, *530*, 71–76.

[62] Yang, Q. S.; Lee, S.; Xue, Y. G.; Yan, Y.; Liu, T. L.; Kang, S. K.; Lee, Y. J.; Lee, S. H.; Seo, M. H.; Lu, D. et al. Materials, mechanics designs, and bioresorbable multisensor platforms for pressure monitoring in the intracranial space. *Adv. Funct. Mater.* **2020**, *30*, 1910718.

[63] Lu, D.; Yan, Y.; Deng, Y. J.; Yang, Q. S.; Zhao, J.; Seo, M. H.; Bai, W. B.; MacEwan, M. R.; Huang, Y. G.; Ray, W. Z. et al. Bioresorbable wireless sensors as temporary implants for *in vivo* measurements of pressure. *Adv. Funct. Mater.* **2020**, *30*, 2003754.

[64] Yu, K. J.; Kuzum, D.; Hwang, S. W.; Kim, B. H.; Juul, H.; Kim, N. H.; Won, S. M.; Chiang, K.; Trumpis, M.; Richardson, A. G. et al. Bioresorbable silicon electronics for transient spatiotemporal mapping of electrical activity from the cerebral cortex. *Nat. Mater.* **2016**, *15*, 782–791.

[65] Hwang, S. W.; Song, J. K.; Huang, X.; Cheng, H. Y.; Kang, S. K.; Kim, B. H.; Kim, J. H.; Yu, S.; Huang, Y. G.; Rogers, J. A. High-performance biodegradable/transient electronics on biodegradable polymers. *Adv. Mater.* **2014**, *26*, 3905–3911.

[66] Hwang, S. W.; Kim, D. H.; Tao, H.; Kim, T. I.; Kim, S.; Yu, K. J.; Panilaitis, B.; Jeong, J. W.; Song, J. K.; Omenetto, F. G. et al. Materials and fabrication processes for transient and bioresorbable high-performance electronics. *Adv. Funct. Mater.* **2013**, *23*, 4087–4093.

[67] Lu, L. Y.; Yang, Z. J.; Meacham, K.; Cvetkovic, C.; Corbin, E. A.; Vázquez-Guardado, A.; Xue, M. T.; Yin, L.; Boroumand, J.; Pakeltis, G. et al. Biodegradable monocrystalline silicon photovoltaic microcells as power supplies for transient biomedical implants. *Adv. Energy Mater.* **2018**, *8*, 1703035.

[68] Zheng, Q.; Zou, Y.; Zhang, Y. L.; Liu, Z.; Shi, B. J.; Wang, X. X.; Jin, Y. M.; Ouyang, H.; Li, Z.; Wang, Z. L. Biodegradable triboelectric nanogenerator as a life-time designed implantable power source. *Sci. Adv.* **2016**, *2*, e1501478.

[69] Li, Y. L.; Maciel, D.; Rodrigues, J.; Shi, X. Y.; Tomás, H. Biodegradable polymer nanogels for drug/nucleic acid delivery. *Chem. Rev.* **2015**, *115*, 8564–8608.

[70] Park, J.; Kim, J. K.; Patil, S. J.; Park, J. K.; Park, S. A.; Lee, D. W. A wireless pressure sensor integrated with a biodegradable polymer stent for biomedical applications. *Sensors* **2016**, *16*, 809.

[71] Hosseini, E. S.; Manjakkal, L.; Shakthivel, D.; Dahiya, R. Glycine–chitosan-based flexible biodegradable piezoelectric pressure sensor. *ACS Appl. Mater. Interfaces* **2020**, *12*, 9008–9016.

[72] Choi, Y. S.; Koo, J.; Lee, Y. J.; Lee, G.; Avila, R.; Ying, H. Z.; Reeder, J.; Hambitzer, L.; Im, K.; Kim, J. et al. Biodegradable polyanhydrides as encapsulation layers for transient electronics. *Adv. Funct. Mater.* **2020**, *30*, 2000941.

[73] Koo, J.; MacEwan, M. R.; Kang, S. K.; Won, S. M.; Stephen, M.; Gamble, P.; Xie, Z. Q.; Yan, Y.; Chen, Y. Y.; Shin, J. et al. Wireless bioresorbable electronic system enables sustained nonpharmacological neuroregenerative therapy. *Nat. Med.* **2018**, *24*, 1830–1836.

[74] Lee, Y. K.; Yu, K. J.; Song, E.; Barati Farimani, A.; Vitale, F.; Xie, Z. Q.; Yoon, Y.; Kim, Y.; Richardson, A.; Luan, H. W. et al. Dissolution of monocrystalline silicon nanomembranes and their use as encapsulation layers and electrical interfaces in water-soluble electronics. *ACS Nano* **2017**, *11*, 12562–12572.

[75] Li, C. Y.; Wu, P. M.; Shutter, L. A.; Narayan, R. K. Dual-mode operation of flexible piezoelectric polymer diaphragm for intracranial pressure measurement. *Appl. Phys. Lett.* **2010**, *96*, 053502.

[76] Warty, R.; Tofighi, M. R.; Kawoos, U.; Rosen, A. Characterization of implantable antennas for intracranial pressure monitoring: Reflection by and transmission through a scalp phantom. *IEEE Trans. Microw. Theory Tech.* **2008**, *56*, 2366–2376.

[77] Won, S. M.; Wang, H. L.; Kim, B. H.; Lee, K.; Jang, H.; Kwon, K.; Han, M. D.; Crawford, K. E.; Li, H. B.; Lee, Y. C. et al. Multimodal sensing with a three-dimensional piezoresistive structure. *ACS Nano* **2019**, *13*, 10972–10979.

[78] Yang, S. X.; Lu, N. S. Gauge factor and stretchability of silicon-on-polymer strain gauges. *Sensors* **2013**, *13*, 8577–8594.

[79] Ying, M.; Bonifas, A. P.; Lu, N. S.; Su, Y. W.; Li, R.; Cheng, H. Y.; Ameen, A.; Huang, Y. G.; Rogers, J. A. Silicon nanomembranes for fingertip electronics. *Nanotechnology* **2012**, *23*, 344004.

[80] Lee, Y. K.; Yu, K. J.; Kim, Y.; Yoon, Y.; Xie, Z. Q.; Song, E. M.; Luan, H. W.; Feng, X.; Huang, Y. G.; Rogers, J. A. Kinetics and chemistry of hydrolysis of ultrathin, thermally grown layers of silicon oxide as biofluid barriers in flexible electronic systems. *ACS Appl. Mater. Interfaces* **2017**, *9*, 42633–42638.

[81] Lee, S. P.; Ha, G.; Wright, D. E.; Ma, Y. J.; Sen-Gupta, E.; Haubrich, N. R.; Branche, P. C.; Li, W. H.; Huppert, G. L.; Johnson, M. et al. Highly flexible, wearable, and disposable cardiac biosensors for remote and ambulatory monitoring. *npj Digital Med.* **2018**, *1*, 2.

[82] Won, S. M.; Song, E. M.; Zhao, J. N.; Li, J. H.; Rivnay, J.; Rogers, J. A. Recent advances in materials, devices, and systems for neural interfaces. *Adv. Mater.* **2018**, *30*, 1800534.

[83] Lee, S.; Inoue, Y.; Kim, D.; Reuveny, A.; Kuribara, K.; Yokota, T.; Reeder, J.; Sekino, M.; Sekitani, T.; Abe, Y. et al. A strain-absorbing design for tissue–machine interfaces using a tunable adhesive gel. *Nat. Commun.* **2014**, *5*, 5898.

[84] Krishnan, S. R.; Ray, T. R.; Ayer, A. B.; Ma, Y. J.; Gutruf, P.; Lee, K. H.; Lee, J. Y.; Wei, C.; Feng, X.; Ng, B. et al. Epidermal electronics for noninvasive, wireless, quantitative assessment of ventricular shunt function in patients with hydrocephalus. *Sci. Trans. Med.* **2018**, *10*, eaat8437.

[85] Kim, J. H.; Kim, S. R.; Kil, H. J.; Kim, Y. C.; Park, J. W. Highly conformable, transparent electrodes for epidermal electronics. *Nano Lett.* **2018**, *18*, 4531–4540.

[86] Jang, T. M.; Lee, J. H.; Zhou, H. L.; Joo, J.; Lim, B. H.; Cheng, H. Y.; Kim, S. H.; Kang, I. S.; Lee, K. S.; Park, E. et al. Expandable and implantable bioelectronic complex for analyzing and regulating real-time activity of the urinary bladder. **2020**, *6*, eabc9675.

[87] Hua, Q. L.; Sun, J. L.; Liu, H. T.; Bao, R. R.; Yu, R. M.; Zhai, J. Y.; Pan, C. F.; Wang, Z. L. Skin-inspired highly stretchable and conformable matrix networks for multifunctional sensing. *Nat. Commun.* **2018**, *9*, 244.

[88] Hannah, S.; Brige, P.; Ravichandran, A.; Ramuz, M. Conformable, stretchable sensor to record bladder wall stretch. *ACS Omega* **2019**, *4*, 1907–1915.

[89] Baik, S.; Lee, H. J.; Kim, D. W.; Kim, J. W.; Lee, Y.; Pang, C. Bioinspired adhesive architectures: From skin patch to integrated bioelectronics. *Adv. Mater.* **2019**, *31*, 1803309.

[90] Wang, Y.; Yu, Y. R.; Guo, J. H.; Zhang, Z. H.; Zhang, X. X.; Zhao, Y. J. Bio-inspired stretchable, adhesive, and conductive structural color film for visually flexible electronics. *Adv. Funct. Mater.* **2020**, *30*, 2000151.

[91] Yao, G.; Yin, C. H.; Wang, Q.; Zhang, T. Y.; Chen, S. H.; Lu, C.; Zhao, K. N.; Xu, W. N.; Pan, T. S.; Gao, M. et al. Flexible bioelectronics for physiological signals sensing and disease treatment. *J. Mater.* **2020**, *6*, 397–413.

[92] Chen, Y.; Zhang, Y. C.; Liang, Z. W.; Cao, Y.; Han, Z. Y.; Feng, X. Flexible inorganic bioelectronics. *npj Flex. Electron.* **2020**, *4*, 2.

[93] Kang, D. Y.; Kim, Y. S.; Ornelas, G.; Sinha, M.; Naidu, K.; Coleman, T. P. Scalable microfabrication procedures for adhesive-integrated flexible and stretchable electronic sensors. *Sensors* **2015**, *15*, 23459–23476.

[94] Han, L.; Lu, X.; Wang, M. H.; Gan, D. L.; Deng, W. L.; Wang, K. F.; Fang, L. M.; Liu, K. Z.; Chan, C. W.; Tang, Y. H. et al. A mussel-inspired conductive, self-adhesive, and self-healable tough hydrogel as cell stimulators and implantable bioelectronics. *Small* **2017**, *13*, 1601916.

[95] Brubaker, C. E.; Messersmith, P. B. Enzymatically degradable mussel-inspired adhesive hydrogel. *Biomacromolecules* **2011**, *12*, 4326–4334.

[96] Yang, Z. L.; Zhao, X.; Hao, R.; Tu, Q. F.; Tian, X. H.; Xiao, Y.; Xiong, K. Q.; Wang, M.; Feng, Y. H.; Huang, N. et al. Bioclickable and mussel adhesive peptide mimics for engineering vascular stent surfaces. *Proc. Natl. Acad. Sci.* **2020**, *117*, 16127–16137.

[97] Baik, S.; Kim, J.; Lee, H. J.; Lee, T. H.; Pang, C. Highly adaptable and biocompatible octopus-like adhesive patches with meniscus-controlled unfoldable 3D microtips for underwater surface and hairy skin. *Adv. Sci.* **2018**, *5*, 1800100.

[98] Lee, H.; Um, D. S.; Lee, Y.; Lim, S.; Kim, H.; Ko, H. Octopus-inspired smart adhesive pads for transfer printing of semiconducting nanomembranes. *Adv. Mater.* **2016**, *28*, 7457–7465.

[99] Baik, S.; Kim, D. W.; Park, Y.; Lee, T. J.; Ho Bhang, S.; Pang, C. A wet-tolerant adhesive patch inspired by protuberances in suction cups of octopi. *Nature* **2017**, *546*, 396–400.

[100] Jin, K. J.; Cremaldi, J. C.; Erickson, J. S.; Tian, Y.; Israelachvili, J. N.; Pesika, N. S. Biomimetic bidirectional switchable adhesive inspired by the gecko. *Adv. Funct. Mater.* **2014**, *24*, 574–579.

[101] Chen, P. J.; Saati, S.; Varma, R.; Humayun, M. S.; Tai, Y. C. Wireless intraocular pressure sensing using microfabricated minimally invasive flexible-coiled LC sensor implant. *J. Microelectromechan. Syst.* **2010**, *19*, 721–734.

[102] Lee, J. O.; Park, H.; Du, J.; Balakrishna, A.; Chen, O.; Sretavan, D.; Choo, H. A microscale optical implant for continuous *in vivo* monitoring of intraocular pressure. *Microsyst. Nanoeng.* **2017**, *3*, 17057.

[103] Lee, J. O.; Narasimhan, V.; Du, J.; Ndjamen, B.; Sretavan, D.; Choo, H. Biocompatible multifunctional black-silicon for implantable intraocular sensor. *Adv. Healthc. Mater.* **2017**, *6*, 1601356.

[104] Narasimhan, V.; Siddique, R. H.; Lee, J. O.; Kumar, S.; Ndjamen, B.; Du, J.; Hong, N.; Sretavan, D.; Choo, H. Multifunctional biophotonic nanostructures inspired by the longtail glasswing butterfly for medical devices. *Nat. Nanotechnol.* **2018**, *13*, 512–519.

[105] Kim, T.; Cho, M.; Yu, K. J. Flexible and stretchable bio-integrated electronics based on carbon nanotube and graphene. *Materials* **2018**, *11*, 1163.

[106] Sang, M. Y.; Shin, J.; Kim, K.; Yu, K. J. Electronic and thermal properties of graphene and recent advances in graphene based electronics applications. *Nanomaterials* **2019**, *9*, 374.

[107] Harris, P. J. F. Carbon nanotube composites. *Int. Mater. Rev.* **2004**, *49*, 31–43.

[108] Avouris, P.; Appenzeller, J.; Martel, R.; Wind, S. J. Carbon nanotube electronics. *Proc. IEEE* **2003**, *91*, 1772–1784.

[109] Robinson, J. T.; Perkins, F. K.; Snow, E. S.; Wei, Z. Q.; Sheehan, P. E. Reduced graphene oxide molecular sensors. *Nano Lett.* **2008**, *8*, 3137–3140.

[110] Compton, O. C.; Nguyen, S. T. Graphene oxide, highly reduced graphene oxide, and graphene: Versatile building blocks for carbon-based materials. *Small* **2010**, *6*, 711–723.

[111] Bai, J. W.; Zhong, X.; Jiang, S.; Huang, Y.; Duan, X. F. Graphene nanomesh. *Nat. Nanotechnol.* **2010**, *5*, 190–194.

[112] Geim, A. K. Graphene: Status and prospects. *Science* **2009**, *324*, 1530–1534.

[113] Dinh, T.; Phan, H. P.; Nguyen, T. K.; Qamar, A.; Woodfield, P.; Zhu, Y.; Nguyen, N. T.; Viet Dao, D. Solvent-free fabrication of biodegradable hot-film flow sensor for noninvasive respiratory monitoring. *J. Phys. D: Appl. Phys.* **2017**, *50*, 215401.

[114] Liao, X. Q.; Liao, Q. L.; Yan, X. Q.; Liang, Q. J.; Si, H. N.; Li, M. H.; Wu, H. L.; Cao, S. Y.; Zhang, Y. Flexible and highly sensitive strain sensors fabricated by pencil drawn for wearable monitor. *Adv. Funct. Mater.* **2015**, *25*, 2395–2401.

[115] Chen, Z. F.; Wang, Z.; Li, X. M.; Lin, Y. X.; Luo, N. Q.; Long, M. Z.; Zhao, N.; Xu, J. B. Flexible piezoelectric-induced pressure sensors for static measurements based on nanowires/graphene heterostructures. *ACS Nano* **2017**, *11*, 4507–4513.

[116] Liu, W. J.; Liu, N. S.; Yue, Y.; Rao, J. Y.; Cheng, F.; Su, J.; Liu, Z. T.; Gao, Y. H. Piezoresistive pressure sensor based on synergistical innerconnect polyvinyl alcohol nanowires/wrinkled graphene film. *Small* **2018**, *14*, 1704149.

[117] Yang, J.; Luo, S.; Zhou, X.; Li, J. L.; Fu, J. T.; Yang, W. D.; Wei, D. P. Flexible, tunable, and ultrasensitive capacitive pressure sensor with microconformal graphene electrodes. *ACS Appl. Mater. Interfaces* **2019**, *11*, 14997–15006.

[118] Zhao, X.; Chen, B.; Wei, G. D.; Wu, J. M.; Han, W.; Yang, Y. Polyimide/Graphene nanocomposite foam-based wind-driven triboelectric nanogenerator for self-powered pressure sensor. *Adv. Mater. Technol.* **2019**, *4*, 1800723.

[119] Park, S. J.; Kim, J.; Chu, M.; Khine, M. J. A. M. T. Flexible piezoresistive pressure sensor using wrinkled carbon nanotube thin films for human physiological signals. *Adv. Mater. Technol.* **2018**, *3*, 1700158.

[120] Boutry, C. M.; Negre, M.; Jorda, M.; Vardoulis, O.; Chortos, A.; Khatib, O.; Bao, Z. A. A hierarchically patterned, bioinspired e-skin able to detect the direction of applied pressure for robotics. *Sci. Robot.* **2018**, *3*, eaau6914.

[121] Nela, L.; Tang, J. S.; Cao, Q.; Tulevski, G.; Han, S. J. Large-area high-performance flexible pressure sensor with carbon nanotube active matrix for electronic skin. *Nano Lett.* **2018**, *18*, 2054–2059.

[122] Jung, S.; Kim, J. H.; Kim, J.; Choi, S.; Lee, J.; Park, I.; Hyeon, T.; Kim, D. H. Reverse-micelle-induced porous pressure-sensitive rubber for wearable human–machine interfaces. *Adv. Mater.* **2014**, *26*, 4825–4830.

[123] Chen, X. Y.; Liu, H.; Zheng, Y. J.; Zhai, Y.; Liu, X. H.; Liu, C. T.; Mi, L. W.; Guo, Z. H.; Shen, C. Y. Highly compressible and robust polyimide/carbon nanotube composite aerogel for high-performance wearable pressure sensor. *ACS Appl. Mater. Interfaces* **2019**, *11*, 42594–42606.

[124] Liu, M. M.; Pu, X.; Jiang, C. Y.; Liu, T.; Huang, X.; Chen, L. B.; Du, C. H.; Sun, J. M.; Hu, W. G.; Wang, Z. L. Large-area all-textile pressure sensors for monitoring human motion and physiological signals. *Adv. Mater.* **2017**, *29*, 1703700.

[125] Xiao, Z. J.; Zhou, W. Y.; Zhang, N.; Zhang, Q.; Xia, X. G.; Gu, X. G.; Wang, Y. C.; Xie, S. S. All-carbon pressure sensors with high performance and excellent chemical resistance. *Small* **2019**, *15*, 1804779.

[126] Lin, J.; Peng, Z. W.; Liu, Y. Y.; Ruiz-Zepeda, F.; Ye, R. Q.; Samuel, E. L. G.; Yacaman, M. J.; Yakobson, B. I.; Tour, J. M. Laser-induced porous graphene films from commercial polymers. *Nat. Commun.* **2014**, *5*, 5714.

[127] Zhu, Y. S.; Cai, H. B.; Ding, H. Y.; Pan, N.; Wang, X. P. Fabrication of low-cost and highly sensitive graphene-based pressure sensors by direct laser scribing polydimethylsiloxane. *ACS Appl. Mater. Interfaces* **2019**, *11*, 6195–6200.

[128] Zhao, T. T.; Li, T. K.; Chen, L. L.; Yuan, L.; Li, X. F.; Zhang, J. H. Highly sensitive flexible piezoresistive pressure sensor developed using biomimetically textured porous materials. *ACS Appl. Mater. Interfaces* **2019**, *11*, 29466–29473.

[129] Mickle, A. D.; Won, S. M.; Noh, K. N.; Yoon, J.; Meacham, K. W.; Xue, Y. G.; McIlvried, L. A.; Copits, B. A.; Samineni, V. K.; Crawford, K. E. et al. A wireless closed-loop system for optogenetic peripheral neuromodulation. *Nature* **2019**, *565*, 361–365.

[130] Yan, D. X.; Bruns, T. M.; Wu, Y. T.; Zimmerman, L. L.; Stephan, C.; Cameron, A. P.; Yoon, E.; Seymour, J. P. Ultracompliant carbon nanotube direct bladder device. *Adv. Healthc. Mater.* **2019**, *8*, 1900477.